Hydrogen evolution reaction

Chapter · June 2003

DOI: 10.1002/9780470974001.f204033

1 author:

Andrzej Lasia
Université de Sherbrooke
199 PUBLICATIONS **11,352** CITATIONS

SEE PROFILE

Hydrogen evolution reaction

A. Lasia

Volume 2, Part 4, pp 416–440

in

Handbook of Fuel Cells – Fundamentals, Technology and Applications
(ISBN: 0-471-49926-9)

Edited by

Wolf Vielstich
Arnold Lamm
Hubert A. Gasteiger

Chapter 29
Hydrogen evolution reaction

A. Lasia

Département de chimie, Université de Sherbrooke, Sherbrooke, Québec, Canada

1 INTRODUCTION

Hydrogen evolution reaction (HER) is one of the most often studied electrochemical processes. It has been known since the 18th century. Although water electrolysis is not the least expensive method of hydrogen production, it supplies hydrogen of a very high purity and is nonpolluting. The total reaction

$$2H_2O_{(l)} \rightleftarrows 2H_{2(g)} + O_{2(g)} \tag{1}$$

arises from a cathodic hydrogen evolution

$$2H_2O + 2e^- \rightleftarrows 2OH^- + H_2 \tag{2}$$

or

$$H^+ + e \rightleftarrows \tfrac{1}{2}H_2 \tag{3}$$

and anodic oxygen evolution reactions

$$4OH^- - 4e^- \rightleftarrows 2H_2O + O_2 \tag{4}$$

or

$$H_2O - 2e \rightleftarrows \tfrac{1}{2}O_2 + 2H^+ \tag{5}$$

More detailed discussion of the mechanism of hydrogen evolution is presented by Manfred Breiter in **Reaction mechanisms of the H_2 oxidation/evolution reaction**, Volume 2. For water electrolysis in alkaline solutions the equilibrium redox potentials of reactions (2)–(5) are

$$E_c = E^0_{H_2} + \frac{RT}{F}\ln\frac{a_{H_2O}}{a_{OH^-}a_{H_2}^{1/2}}$$

or (6)

$$E_c = E^0_{H_2} + \frac{RT}{F}\ln\frac{a_{H^+}}{a_{H_2}^{1/2}}$$

and

$$E_a = E^0_{O_2} + \frac{RT}{F}\ln\frac{a_{O_2}^{1/4}a_{H_2O}^{1/2}}{a_{OH^-}}$$

or (7)

$$E_a = E^0_{O_2} + \frac{RT}{F}\ln\frac{a_{O_2}^{1/4}a_{H^+}^{1/2}}{a_{H_2O}}$$

and the equilibrium potential for water electrolysis is

$$E = E^0_{O_2} - E^0_{H_2} + \frac{RT}{F}\ln\left(\frac{p_{O_2}^{1/4}p_{H_2}^{1/2}}{a_{H_2O}^{1/2}}\right)$$

$$= E^0_{H_2O} + \frac{RT}{2F}\ln\left(\frac{p_{O_2}^{1/2}p_{H_2}}{a_{H_2O}}\right) \tag{8}$$

The standard potentials of reactions (6) and (7) in alkaline solutions are: $E^0_{H_2} = -0.828\,V$ and $E^0_{O_2} = 0.401\,V$ versus normal hydrogen electrode (NHE) at 25 °C. This means, that the reversible voltage for reaction (1) is $E^0_{H_2O} = 1.229\,V$, which is equivalent to $\Delta G^0 = -2F(-E^0_{H_2O}) = 237.2\,kJ\,mol^{-1}$ at 25 °C. This value is independent of the solution pH. The thermodynamic parameters of reaction (1)

Handbook of Fuel Cells – Fundamentals, Technology and Applications, Edited by Wolf Vielstich, Hubert A. Gasteiger, Arnold Lamm. Volume 2: *Electrocatalysis*. © 2003 John Wiley & Sons, Ltd. ISBN: 0-471-49926-9.

are:[1] $\Delta G^0 = 237.178\,\mathrm{kJ\,mol^{-1}}$, $\Delta H^0 = 285.830\,\mathrm{kJ\,mol^{-1}}$ and $\Delta S^0 = 163.18\,\mathrm{J\,mol^{-1}\,K^{-1}}$ (per mole of hydrogen) at 25 °C. This indicates, that for electrolysis at the reversible electrode potential thermal energy $285.830 - 237.178 = 48.652\,\mathrm{kJ\,mol^{-1}}$ must be supplied from the surroundings to carry out water electrolysis at 25 °C. Only applying electrical energy equivalent to $\Delta H^0 = 285.830\,\mathrm{kJ\,mol^{-1}}$ that is $E^{0,\mathrm{en}}_{\mathrm{H_2O}} = 1.481\,\mathrm{V}$ water will be electrolyzed isothermally. This is called enthalpic voltage, and decreases slowly with the increase in temperature according to[2]

$$E^{0,\mathrm{en}}_{\mathrm{H_2O}} = 1.4850 - 1.490 \times 10^{-4} t - 9.84 \times 10^{-8} t \ (\mathrm{V}) \quad (9)$$

where t is temperature in °C. It may be noted that with the increase of the temperature, the standard water electrolysis voltage decreases:[2]

$$E^0_{\mathrm{H_2O}}(T) = 1.5184 - 1.5421 \times 10^{-3} T + 9.523 \times 10^{-5} T \ln T + 9.84 \times 10^{-8} T^2 \ (\mathrm{V}) \quad (10)$$

By increasing the pressure the reversible potential increases, as the gases produced must be compressed:[3]

$$E_{\mathrm{H_2O},p} = E^0_{\mathrm{H_2O},p=1} + \frac{RT}{2F} \ln \frac{(p - p_{\mathrm{H_2O}})^{1.5}}{(p_{\mathrm{H_2O}}/p^0_{\mathrm{H_2O}})} \quad (11)$$

where p is the pressure at which the electrolysis takes place (assuming pure O_2 and H_2 on both sides of the cell), $p_{\mathrm{H_2O}}$ and $p^0_{\mathrm{H_2O}}$ are the water vapor pressure over the electrolyte and over pure water. At 120 °C and 35 atm the electrolysis voltage is increased by ~90 mV and this value should be added to the standard cell potential.

In practice water must be heated up to the electrolysis temperature and water vapor leaves the cell together with H_2 and O_2. Taking into account additional energy connected with water, so-called thermoneutral water electrolysis voltage, $E^{\mathrm{tn}}_{\mathrm{H_2O}}$ is obtained. It is expressed as the sum of the enthalpic voltage, $E^{0,\mathrm{en}}_{\mathrm{H_2O}}$, energy necessary to heat water from 25 °C to temperature t, $(\tilde{H}^0_t - \tilde{H}^0_{25})_{\mathrm{w(l)}}$ and energy of production of steam over the electrolytic solution:[2]

$$E^{\mathrm{tn}}_{\mathrm{H_2O}} = E^{0,\mathrm{en}}_{\mathrm{H_2O}} + \frac{(\tilde{H}^0_t - \tilde{H}^0_{25})_{\mathrm{w(l)}}}{2F} + 1.5 \frac{p_{\mathrm{w}}}{p - p_{\mathrm{w}}} \frac{\tilde{H}_{\mathrm{w(g)},t,p} - \tilde{H}_{\mathrm{w(l)},25}}{2F} \quad (12)$$

where w(l) and w(g) denote liquid and gaseous water and $\tilde{H}_i$ are the partial molar enthalpies of the species i. The first and second terms represent so-called higher heating value voltage, $E^{0,\mathrm{HHV}}_{\mathrm{H_2O}}$

$$E^{0,\mathrm{HHV}}_{\mathrm{H_2O}} = E^{0,\mathrm{en}}_{\mathrm{H_2O}} + \frac{(\tilde{H}^0_t - \tilde{H}^0_{25})_{\mathrm{w(l)}}}{2F} = 1.4756 + 2.252 \times 10^{-4} t + 1.52 \times 10^{-8} t^2 \ (\mathrm{V}) \quad (13)$$

and the last term may be described as

$$\tilde{H}_{\mathrm{w(g)},t,p} - \tilde{H}_{\mathrm{w(l)},25} = 42\,960 + 40.762t - 0.06682t^2 \ (\mathrm{J\,mol^{-1}}) \quad (14)$$

An example of dependence of these potentials as a function of temperature for standard conditions and for 30% KOH at 25 atm is displayed in Figure 1. In practical applications additional heat losses (due to radiation, convection, conduction) must also be added to the heat balance.

The practical voltage applied to carry out water electrolysis is larger than the thermodynamic values calculated above. It is expressed as

$$E = E^{\mathrm{tn}}_{\mathrm{H_2O}} + \eta_{\mathrm{a}} + \eta_{\mathrm{c}} + iR \quad (15)$$

where η_{a} and η_{c} are anodic and cathodic overpotentials, respectively, i is the circulating current and R is the electrical resistance of the solution, electrodes and electrical leads. Of course one cannot avoid thermodynamic constraints, which in the case of water electrolysis are very costly.

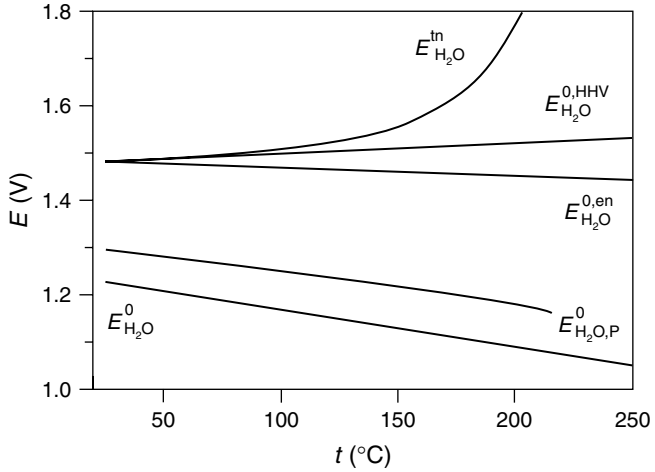

Figure 1. Variation of various voltages for water electrolysis as functions of temperature in standard conditions and in 30% KOH at the pressure of 25 atm: standard cell voltage, $E^0_{\mathrm{H_2O}}$, reversible at $p = 35$ atm, $E_{\mathrm{H_2O},p}$, enthalpic, $E^{0,\mathrm{en}}_{\mathrm{H_2O}}$, higher heating value, $E^{0,\mathrm{HHV}}_{\mathrm{H_2O}}$ and thermoneutral, $E^{\mathrm{tn}}_{\mathrm{H_2O}}$.

By better construction engineering (cell construction, membranes) it is possible to reduce the ohmic drop, iR, and the *main effort of electrocatalysis is to reduce overpotentials*. There are two ways to improve the electrode performance:

(1) use of electrode materials characterized by higher intrinsic activity i.e., higher exchange current density;
(2) use of electrode materials characterized by large real surface area.

In general, electrodes may be characterized by the Tafel parameters: exchange current density, j_0, and the slope, b; for the most active electrodes the former should be the largest, the latter the smallest. There are, however, several problems with these parameters. Firstly, the electrode real surface area is rarely known and j_0 is expressed per geometric surface area. In such a case comparison of intrinsic activities is impossible. Secondly, complex reaction mechanism and the use of porous electrodes lead to nonlinear Tafel plots and the extrapolation of j_0 is not reliable. Therefore, there exists another experimental parameter characterizing a given electrode in the working condition: overpotential at a specified apparent current density, e.g., η_{100}, η_{250} or η_{500} which correspond to the overpotential at an apparent (with respect to the geometrical surface area) current density of 100, 250 and 500 mA cm^{-2}. Water electrolysis is usually carried out in 25–50% KOH at 70–90 °C. Industrial electrodes should possess long-time stability, both physical (physical disintegration) and electrochemical (keep their activity, immune to contamination) and be immune to the current interruptions and short circuit i.e., exposition in the solution under the open circuit conditions.

The best materials for hydrogen evolution are noble metals: Pt, Rh or Ru. Of course these materials cannot be used directly as solid metals for industrial processes because of their high cost. Industrial hydrogen evolution was initially carried out on mild steel and nickel electrodes. Newer active electrode materials have been gradually developed and introduced; however, lack of proper scale-up practice is one of the primary drawbacks of the present technology. There are several books and reviews on the materials for hydrogen evolution,[4–8] and it is impossible to describe all the literature in this review. Below, a short survey of various electrode materials is presented, mainly based on more recent works.

It is generally accepted that the HER may proceed through three steps in acid and alkaline solutions, respectively:

(1) electrochemical hydrogen adsorption, Volmer reaction

$$H^+ + M + e \underset{\vec{k}_1}{\overset{k_{-1}}{\rightleftharpoons}} MH_{ads} \qquad (16)$$

or

$$H_2O + M + e \underset{\vec{k}_1}{\overset{k_{-1}}{\rightleftharpoons}} MH_{ads} + OH^- \qquad (17)$$

followed by

(2) electrochemical desorption, Heyrovsky reaction

$$MH_{ads} + H^+ + e \underset{\vec{k}_2}{\overset{k_{-2}}{\rightleftharpoons}} M + H_2 \qquad (18)$$

or

$$MH_{ads} + H_2O + e \underset{\vec{k}_2}{\overset{k_{-2}}{\rightleftharpoons}} M + OH^- + H_2 \qquad (19)$$

(3) chemical desorption, Tafel reaction

$$2MH_{ads} \underset{k_3}{\overset{k_{-3}}{\rightleftharpoons}} 2M + H_2 \qquad (20)$$

The steady-state current for Volmer–Heyrovsky reaction mechanism is described in acid solutions by the following equation:

$$j = 2F \frac{k_1 k_2 e^{-\beta f \eta} \left[\left(\frac{a_{H^+}}{a_{H^+,0}} \right)^2 - \left(\frac{a_{H_2}}{a_{H_2,0}} \right) e^{2f\eta} \right]}{(k_1 + k_2) \left(\frac{a_{H^+}}{a_{H^+,0}} \right) + \left[k_{-1} + k_{-2} \left(\frac{a_{H_2}}{a_{H_2,0}} \right) \right] e^{f\eta}} \qquad (21)$$

where β is the transfer coefficient, η overpotential, $f = F/RT$ and index 0 denotes concentration at the equilibrium potential. Assuming that there is no concentration polarization of H^+

$$j = 2F \frac{k_1 k_2 e^{-\beta f \eta} \left[1 - \left(\frac{a_{H_2}}{a_{H_2,0}} \right) e^{2f\eta} \right]}{(k_1 + k_2) + \left[k_{-1} + k_{-2} \left(\frac{a_{H_2}}{a_{H_2,0}} \right) \right] e^{f\eta}} \qquad (22)$$

In the basic solutions this equation is[9]

$$j = 2F \frac{k_1 k_2 e^{-\beta f \eta} \left[\left(\frac{a_{H_2O}}{a_{H_2O,0}} \right)^2 - \left(\frac{a_{OH^-}}{a_{OH^-,0}} \right)^2 \left(\frac{a_{H_2}}{a_{H_2,0}} \right) e^{2f\eta} \right]}{k_1 \left(\frac{a_{H_2O}}{a_{H_2O,0}} \right) + k_2 \left(\frac{a_{H_2O}}{a_{H_2O,0}} \right) + \left[k_{-1} \left(\frac{a_{OH^-}}{a_{OH^-,0}} \right) + k_{-2} \left(\frac{a_{OH^-}}{a_{OH^-,0}} \right) \left(\frac{a_{H_2}}{a_{H_2,0}} \right) \right] e^{f\eta}} \qquad (23)$$

or assuming that the concentration of OH^- and water is not affected by direct current (d.c.)

$$j = 2F \frac{k_1 k_2 e^{-\beta f \eta} \left[1 - \left(\frac{a_{H_2}}{a_{H_2,0}} \right) e^{2 f \eta} \right]}{k_1 + k_2 + \left[k_{-1} + \left(\frac{a_{H_2}}{a_{H_2,0}} \right) k_{-2} \right] e^{f \eta}} \quad (24)$$

The effects of the hydrogen concentration gradient may be observed only at very active noble electrodes at lower overpotentials. Assuming transfer coefficients, $\beta = 0.5$, and Langmuir adsorption isotherm the Volmer–Heyrovsky mechanism gives Tafel slopes of $\ln 10\ RT/(1+\beta)F = 39.4\,\text{mV dec}^{-1}$ and $\ln 10\ RT/\beta F = 118.3\,\text{mV dec}^{-1}$ at 25 °C.

For Volmer–Tafel mechanism at low hydrogen surface coverages and limitations by Tafel reaction current is described as

$$j = 2F k_{-3} e^{-2 f \eta} \quad (25)$$

which gives slope of $\ln 10\ RT/2F = 29.6\,\text{mV dec}^{-1}$ at 25 °C. When the whole process is limited by Volmer reaction the slope is $\ln 10\ RT/\beta F = 118.3\,\text{mV dec}^{-1}$. At high overpotentials when the process is limited by the rate of chemical reaction[20] current becomes independent of overpotential and the Tafel slope becomes infinite. In many cases intermediary slopes are observed which may indicate Frumkin/Temkin adsorption isotherm. On very porous electrodes a doubling of Tafel plots may be observed.

2 HYDROGEN EVOLUTION ON POLYCRYSTALLINE METALS

It is well known that the activity of the electrode material towards the HER depends on its electronic structure. Plot of the exchange current density versus atomic number of the element (Gchhneidner relation[10]) shows periodic appearance of volcano-type curves.[11] Parsons[12] has shown that the kinetics of the HER is related to the ΔG^0_H of hydrogen adsorption on the electrode surface. The rate constants for Volmer and Heyrovsky reaction may be expressed as $k_i = k_i^0 \exp[-\beta_i(\Delta G^0_H/RT)]$ for forward and $k_{-i} = k_{-i}^0 \exp[(1-\beta_i)(\Delta G^0_H/RT)]$ for the backward reactions, respectively,[13] therefore, the chemical nature of the surface influences the kinetics of the HER. Trasatti[14] plotted logarithm of the exchange current densities for the HER, log j_0, on different metals, against the metal–hydrogen, M–H, bond strength. This relation, displayed in Figure 2,[15] represents so-called volcano curve

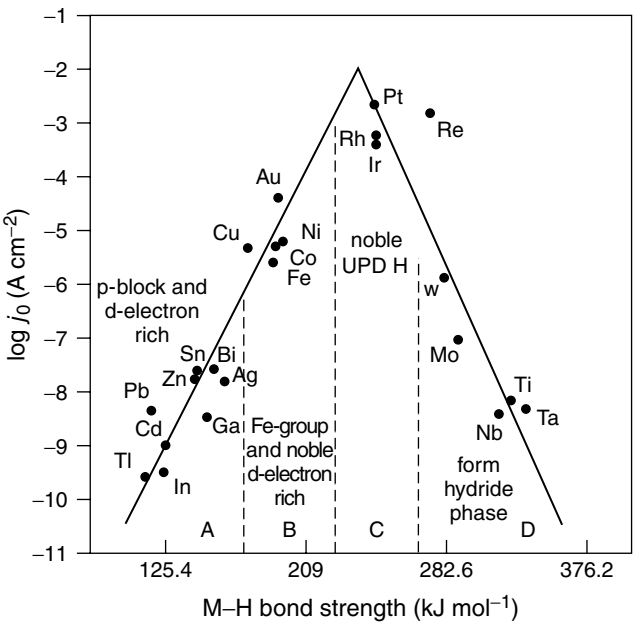

Figure 2. Experimental volcano plot of the standard exchange current density, log j_0, versus M–H bond energy on different metals.[15] (Reproduced from Conway and Jerkiewicz (2000)[15] with permission from Elsevier Science.)

with the maximum corresponding to the platinum group metals. It permits for a quick comparison of the activities of different metals. However, there are several problems with this approach. First, the exchange current densities can be compared only for the same reaction mechanisms but, in fact, HER mechanisms are different for different metals (e.g., as evidenced by different Tafel slopes).[16] Moreover, the kinetic data used for construction of this plot were determined in different experimental conditions and even in acidic and alkaline solutions. They were not always obtained in very pure electrolytes and various data exist in the literature for the same metals (contamination decreases the kinetics). The state of the electrode surface in solution is also different for different metals: some metals form stable oxides and/or hydrides. On certain noble metals two types of hydrogen coexist, underpotential and overpotential H (OPD H) and the HER takes place on the surface covered by the underpotential hydrogen, UPH H.[15] Only weakly adsorbed OPD H is involved in the HER but the adsorption energies used correspond to the UPD process. Moreover, the M–H bond energies were taken from the gas phase reactions referred to the zero coverage. Despite all these problems the volcano relation is a useful way for experimental comparison of the activities. However, more experimental research is necessary to obtain good quality experimental data. Relations with other parameters have been proposed for the HER[16] but, up to now, it is only possible to suggest a tendency for the

exchange current densities without giving any quantitative relationship. A more practical parameter characterizing the apparent electrode activity than the exchange current itself is the overpotential at a given current density.[17]

The most active metals for the HER are platinum group metals (Pt, Re, Rh, Ir) followed by transition metals (Au, Ni, Co, Fe, Cu). For the most active metals fast deactivation is often observed due to adsorption or electrodeposition of impurities. Determination of the detailed kinetics of the HER is still continuing and with improvements in preparation of very clean surfaces and solutions, new data are being obtained showing even higher activities than those found earlier. However, discrepancies between different authors still exist. More studies are necessary to obtain better experimental results and, subsequently, more reliable kinetic data. On the other end, Hg is one of the least active materials (see Table 1). Graphite is also quite inactive material but important increase in the activity was found after argon plasma etching.[18] Many experimental data for various metals are given in Refs. [4, 5]. Some more recent results are shown in Table 1 and more detailed results for Pt and Ni are presented below.

2.1 Platinum

Platinum is one of the most active and most frequently studied metals. The exchange current density in H_2SO_4 is 5×10^{-4} to $10^{-3}\,A\,cm^{-2}$ and the Tafel slope of $30\,mV\,dec^{-1}$ at low overpotentials[5] and $120\,mV\,dec^{-1}$ at high overpotentials[19] or only one slope of $29\,mV\,dec^{-1}$ with $j_0 = 10^{-3}\,A\,cm^{-2}$[20] is observed. This indicates Volmer–Tafel mechanism at low and Volmer–Heyrovsky mechanism at higher overpotentials. More detailed studies have recently been conducted on monocrystalline electrodes. It was found that the mechanism and kinetics of the HER depend strongly on the crystal face orientation.[20–22] Barber *et al.*[20] have found that the activity decreases in the order: Pt(110) > Pt(111) > Pt(100) cooled in $H_2 + Ar$, while Marković *et al.*[22] found order Pt(110) > Pt(100) > Pt(111). Low Tafel slopes observed at the rotating disk electrode were attributed to the limitations by H_2 diffusion from electrode.[20] Rate constants of the HER are shown in Table 2.

The activity of Pt depends on the size of its crystallites.[23] Studies of the deposition of Pt nanocrystallites (40–50 nm) on Ti show that the specific activity of these crystallites is three times higher than that of the polycrystalline Pt electrode. Because of the large surface area of the nanocrystallites, the apparent activity is thousands of times larger. Comparison of activities of various Pt electrodes is presented in Table 1.

It has been suggested that alkali metal ions might deposit on the metal surfaces in alkaline solutions.[24, 25]

2.2 Nickel

Nickel and nickel-based electrodes are among the best materials for water electrolysis in alkaline media because of their relatively high activity and chemical stability. The kinetics of the HER depends on the purity of solutions and traces of Fe (0.5 ppm) usually found in alkaline solutions decrease the electrode activity.[26] However, studies of a very intensive HER at $2\,A\,cm^{-2}$ in the presence of 14 ppm of Fe displayed increase in the electrocatalytic activity due to deposition of porous Fe and increase in surface roughness.[27] It was also found that even in the purest (preelectrolyzed) NaOH solutions and in a polysulfone cell some deposition of metallic contaminants (mainly Fe) occurs, decreasing the electrode activity during water electrolysis.[28] Therefore, it is very difficult to determine the kinetics of HER in alkaline solutions. Addition of EDTA to the alkaline solution prevents electrode deactivation by complexing metallic ions and displacing their reduction potential to more negative values.[29, 30] However, at more negative potentials deposition of iron is always observed.[31] Formation of a subsurface hydride on Ni was found during intensive HER.[32–34] It was also suggested that this hydride might inhibit HER.

Kinetics and mechanism of HER on Ni have been studied in detail by Lasia and Rami[35] and Hitz and Lasia.[30, 36] The Tafel parameters of the HER on Ni are displayed in Table 1. HER proceeds through the Volmer–Heyrovsky mechanism and the rate constants are displayed in Table 2. The same values of rate constants were obtained using electrochemical impedance spectroscopy, galvanostatic pulse and open circuit potential decay methods.[36] Double layer capacitance of Ni electrode was $42\,\mu F\,cm^{-2}$, which indicates low surface roughness.[30, 36]

To increase the apparent electrode activity, the real surface area was increased by using screen or whisker electrodes,[37] sintered Ni powder on porous nickel,[38, 39] or pressed Ni powders[40] (see Table 1). In situ activation of Ni and Co electrodes in 30% KOH was observed after addition of sodium molybdenate, which was attributed to deposition of metallic Mo on the electrode surface.[41] Similarly, addition of dissolved V_2O_5 reactivates Ni cathodes for the HER by deposition of metallic vanadium.[42]

Kreysa *et al.*[43] studied HER on Ni in 1 M KOH. They found existence of a limiting current of $\geq 1\,A\,cm^{-2}$ at high

Table 1. Activities of selected metals towards the HER; b Tafel slope, j_0 exchange current density, η_j overpotential at the current density of j mA cm^{-2}.

Electrode	Conditions	b (mV dec^{-1})	Activity	Ref.
Pt polycrystalline	0.5 M H_2SO_4, 23 °C; anodically activated after cathodic polarization	36, 68 and 125	$j_0 = 3.2° \times 10^{-3}$ A cm^{-2}; $j_0 = 1.6° \times 10^{-3}$ A cm^{-2}	[260]
Pt polycrystalline	0.5 M H_2SO_4	29	$j_0 = 10^{-3}$ A cm^{-2}; $\eta_{250} = 60$ mV	[20]
Pt polycrystalline	0.5 M NaOH, 23 °C; anodically activated after cathodic polarization	75 mV; 125	$j_0 = 3.1 \times 10^{-4}$ A cm^{-2}; $j_0 = 4.4 \times 10^{-5}$ A cm^{-2}	[260]
Pt(110)	0.05 M H_2SO_4, 30 °C		$j_0 = 9.8 \times 10^{-4}$ A cm^{-2}	[22]
Pt(100)	0.05 M H_2SO_4, 30 °C		$j_0 = 6 \times 10^{-4}$ A cm^{-2}	[22]
Pt(111)	0.05 M H_2SO_4, 30 °C		$j_0 = 4.5 \times 10^{-4}$ A cm^{-2}	[22]
Ir	0.5 M H_2SO_4, 25 °C	35	$j_0 = 2.5 \times 10^{-4}$ A cm^{-2}; $\eta_{10} = 56$ mV	[261]
Rh	1 M KOH, 25 °C; 1 M KOH, 75 °C	190; 164	$j_0 = 5.5 \times 10^{-4}$ A cm^{-2}; $j_0 = 7.8 \times 10^{-3}$ A cm^{-2}	[262]
Au	1 M H_2SO_4, 21 °C	103	$j_0 = 1.4 \times 10^{-6}$ A cm^{-2}	[263]
Au	1 M HCl, 20 °C	99	$j_0 = 1.5 \times 10^{-10}$ A cm^{-2}	[263]
Au	0.5 M NaOH, 23 °C	120	$j_0 = 5.6 \times 10^{-6}$ A cm^{-2}	[264]
Ag	1 M H_2SO_4, 20 °C	100	$j_0 = 1.9 \times 10^{-10}$ A cm^{-2}	[263]
Cu	1 M H_2SO_4, 21 °C	105	$j_0 = 5.6 \times 10^{-8}$ A cm^{-2}	[263]
Ni polycrystalline	1 M NaOH, 25 °C; 1 M NaOH, 70 °C	119; 114	$j_0 = 5.0 \times 10^{-5}$ A cm^{-2}; $j_0 = 5.6 \times 10^{-5}$ A cm^{-2}	[36]
Ni polycrystalline	30% KOH, 28 °C	80 low d.c.; 160 high cd	$j_0 = 6 \times 10^{-5}$ A cm^{-2}; $j_0 = 2.1 \times 10^{-3}$ A cm^{-2}; $\eta_{250} = 345$ mV	[44]
Ni polycrystalline	30% KOH, 77 °C	80 low d.c.; 166 high cd	$j_0 = 4.1 \times 10^{-4}$ A cm^{-2}; $j_0 = 9.3 \times 10^{-3}$ A cm^{-2}; $\eta_{250} = 253$ mV	[44]
Ni polycrystalline	50% KOH, 80 °C	140	$j_0 = 1.1 \times 10^{-4}$ A cm^{-2}	[47]
Ni polycrystalline	50% KOH, 264 °C	66 low cd; 200 high cd	$j_0 = 9.3 \times 10^{-4}$ A cm^{-2}; $j_0 = 2.0 \times 10^{-2}$ A cm^{-2}	[47]
Ni electrodeposited	28% KOH, 25 °C	184	$j_0 = 1.3 \times 10^{-4}$ A cm^{-2}; $\eta_{135} = 579$ mV	[48]
Ni electrodeposited; impregnated with molybdenite	28% KOH, 25 °C	64	$j_0 = 3.6 \times 10^{-4}$ A cm^{-2}; $\eta_{135} = 188$ mV	[48]
Ni electrodeposited; impregnated with MoS_2	28% KOH, 25 °C	52	$j_0 = 1.8 \times 10^{-4}$ A cm^{-2}; $\eta_{135} = 138$ mV	[48]
Ni electrodeposited; impregnated with MoS_2	28% KOH, 80 °C	48	$j_0 = 3.4 \times 10^{-4}$ A cm^{-2}; $\eta_{135} = 134$ mV; $\eta_{250} = 244$ mV	[48]
Ni pressed powder	1 M NaOH, 70 °C	180	$j_0 = 1.1 \times 10^{-3}$ A cm^{-2}; $\eta_{250} = 426$ mV	[40]
Co	H_2SO_4, pH = 0.95	140	$j_0 = 3.6 \times 10^{-6}$ A cm^{-2}	[265]
Co	NaOH, pH = 12.9	145	$j_0 = 5.5 \times 10^{-6}$ A cm^{-2}	[265]
Fe	0.05 M H_2SO_4 + 0.45 M Na_2SO_4	$\alpha = 0.5$	$j_0 = 2 \times 10^{-6}$ A cm^{-2}	[266]
Fe	0.1 M KOH		$\eta_{10} = 0.44$ V	[267]
Fe	2 M NaOH, 20 °C; 2 M NaOH, 60 °C	133; 156	$j_0 = 9.1 \times 10^{-6}$ A cm^{-2}; $\eta_{10} = 510$ mV; $j_0 = 1.7 \times 10^{-4}$ A cm^{-2}; $\eta_{10} = 360$ mV	[268]
Fe electrodeposited	28% KOH; 24 °C; 80 °C	83 low c.d.; 115 high c.d.; 36 low c.d.; 120 high c.d.	$\eta_{135} = 248$ mV; $\eta_{135} = 119$ mV	[269]

(*continued overleaf*)

Table 1. (*continued*)

Electrode	Conditions	b (mV dec^{-1})	Activity	Ref.
W	KOH, pH = 13.54, 25 °C	73 low CD; 110 high CD	$j_0 = 1.8 \times 10^{-8}$ A cm^{-2}; $j_0 = 9.2 \times 10^{-7}$ A cm^{-2}	[270]
W electrodeposited	KOH, pH = 13.54, 25 °C	85 low CD; 122 high CD	$j_0 = 3.5 \times 10^{-7}$ A cm^{-2}; $j_0 = 2.0 \times 10^{-6}$ A cm^{-2}	[270]
Hg	0.5 M H_2SO_4, 20 °C	116	$\eta_1 = 1010$ mV	[271]

Table 2. Kinetic parameters of the HER on Pt and Ni.

Electrode	k_1 (mol s^{-1} cm^{-2})	k_{-1} (mol s^{-1} cm^{-2})	k_2 or k_3 (mol s^{-1} cm^{-2})	Ref.
Pt(111), 0.5 M H_2SO_4	4.6×10^{-5}	1.4×10^{-4}	$k_3 = 3.9 \times 10^{-6}$	[20]
Pt(511), 0.5 M H_2SO_4	3.2×10^{-6}	5.1×10^{-5}	$k_3 = 7.9 \times 10^{-5}$	[20]
Pt(100), 0.5 M H_2SO_4, cooled in air	1.3×10^{-5}	8.8×10^{-5}	$k_3 = 1.1 \times 10^{-5}$	[20]
Pt(100), 0.5 M H_2SO_4, cooled in H_2 + Ar	8.7×10^{-7}	7.7×10^{-6}	$k_3 = 3.1 \times 10^{-6}$	[20]
Pt polycrystalline, 0.5 M H_2SO_4	8.9×10^{-7}	4.8×10^{-5}	$k_2 = 3.4 \times 10^{-5}$; $k_3 = 5.9 \times 10^{-13}$	[272]
Pt(110), 0.5 M NaOH	6×10^{-5}	10^{-4}	$k_3 = 9 \times 10^{-5}$	[20]
Pt polycrystalline, 0.5 M NaOH, 23 °C	4.4×10^{-8}	4.4×10^{-7}	$k_2 = 2.4 \times 10^{-9}$; $k_3 = 8.8 \times 10^{-8}$	[273]
Pt polycrystalline, 0.5 M NaOH, anodically activated	10^{-8}	3×10^{-7}	$k_2 = 2 \times 10^{-10}$; $k_3 = 2.8 \times 10^{-8}$	[274]
Ni polycrystalline, 1 M NaOH, 25 °C	3.0×10^{-8}	3.3×10^{-7}	$k_2 = 1.1 \times 10^{-11}$	[36]

overpotentials (>0.6 V) and attributed it to the limitations by the Tafel reaction. Other studies[44, 45] do not confirm such limitations, which indicates that the plateau obtained was due to the uncompensated *IR* drop in cell. Dependence of the activity of on crystallographic surface orientation was found, with Ni(100) being most active and Ni(111) the least active.[46]

Studies of Ni in the industrial electrolysis conditions have revealed two Tafel slopes.[44] Studies at higher temperatures and pressures in 50% KOH revealed one Tafel slope at 80 °C and two Tafel slopes at higher temperatures: 54–70 mV dec^{-1} at lower and 200–320 at higher overpotentials.[47] Large increase in electrocatalytic activity of Ni was observed at higher temperatures. Addition of natural molybdenate (MoS_2) or synthetic MoS_2 during electrodeposition of Ni significantly increases the electrode activity and decreases the Tafel slope[48] (Table 1, see also Section 5.5).

3 HYDROGEN EVOLUTION ON ALLOYS, INTERMETALLIC COMPOUNDS AND COMPOSITES

Alloying various metals often leads to an increase in electrocatalytic activity. The Brewer–Engel theory[49] predicts that for alloys and intermetallic compounds a maximum in bond strength and stability is expected when metals of the left half of the transition series, having empty or half-filled vacant d-orbitals, are alloyed with metals of the right half of the transition series having internally paired d-electrons

not available for bonding in pure metals. Jakšić[11, 50, 51] has applied this theory to predict and explain enhanced activity towards the HER of several alloys and intermetallic compounds (Cr_3Si, $MoCo_3$, WNi_3, $HfPd_3$, VNi_3, Ti/Ni, Zr/Ni, Mo/Ni, Mo/Pt etc.). However, other studies did not find any relation with % d-character.[52] The Brewer–Engel theory applies to bulk properties of solids while the electrocatalytic activity depends on the surface properties, which are not simply related to bulk properties. Moreover, surface roughness very often contributes more to the global electrocatalytic activity than the intrinsic activity. More detailed and good quality experimental studies are necessary to check theoretical predictions.[7]

Industrial HER has been traditionally carried out on mild steel in alkaline media. Tafel plots on this material show two regions with the same Tafel slope $\sim 120\,\text{mV dec}^{-1}$ but with the discontinuity at $\sim 30\,\text{mA cm}^{-2}$.[53] Much higher activities may be obtained by alloying Ni with Fe. As Ni electrode is easily poisoned by traces of Fe, such an alloy would be immune to poisoning by this element. Two Tafel slopes are produced on Ni/Fe alloys and the overpotential η_{135} is 244 mV smaller than that on mild steel. The activity is partially related to the surface roughness.

3.1 Ni/Mo

One of the most studied alloys is Ni/Mo. Brown *et al.*[54, 55] have prepared these materials by thermal decomposition of metallic salts followed by reduction in hydrogen atmosphere and reported overpotential $\eta_{1000} = 83\,\text{mV}$ for Ni/Mo (30–70%). This alloy may also be prepared by electrodeposition.[56] Divisek *et al.*[57] have compared several methods of production of Ni/Mo coatings and found that Mo is leached out from the deposit and deactivation is observed after current interruption for several hours. Certain methods of preparation produce oxides which influence electrocatalytic activity. Very active electrodes have been obtained by ball milling of metallic powders.[58] The electrocatalytic properties correlate directly with the size of the crystallites; a linear relation exists between the HER overpotential and crystal size, while arc melted polycrystalline alloys are not very active (Table 3). Ni/Mo alloys prepared by mechanical alloying and subsequent consolidation are also active for the HER.[59] Cold pressed electrodes were more active than hot pressed ones. During hot pressing, multiphase systems were produced ($Ni_4Mo + MoO_2$). Nanocrystalline $Ni_{80}Mo_{20}$ alloy was more active than the amorphous $Ni_{57}Mo_{43}$.

Comparison of metallurgically prepared pure Ni/Mo phases have revealed that the activity decreases in the order NiMo > Ni_2Mo > Ni_3Mo > Ni_4Mo.[60] As it can be seen from Table 3 these materials are not very active, with $\eta_{100} = 420\,\text{mV}$ for NiMo. This means that the method of preparation, high surface area and the presence of oxides may play a very important role in the overall electrode activity.

Modification of the NiMo alloy by introduction of Cd increases the activity remarkably. A patented method has been developed to electrodeposit $Ni_{79}Mo_{20}Cd_1$.[61] It produces highly active electrodes characterized by two Tafel slopes and $\eta_{100} \sim 140\,\text{mV}$.[62] The deposit is characterized by high surface roughness (roughness factor ~900).[63] Several other Ni/Mo alloys doped by other metals were prepared by electroplating technique.[64] It was found that the electrocatalytic activity towards hydrogen evolution decreases in order: Ni/Mo/Fe > Ni/Mo/Cu > Ni/Mo/Zn > Ni/Mo/W~Ni/Mo/Co > Ni/Mo/Cr.

3.2 Other alloys

Ni/Sn alloys have been studied by several authors.[52, 65, 66] Conflicting results have been reported. Metallurgically prepared samples were not very active[52] but electrodeposited alloys were active.[65, 66] The highest activity was observed for samples containing ~50% of Sn, they were characterized by the surface roughness of 74. Electrocatalytic activity decreased with increase of the crystallite size and the most active electrode had crystallite seize if 5 nm.

Electrodeposited $Ni_{150}Mn_{50}Fe_{10}$ coatings have an optimal composition for the HER.[67] A number of other alloys prepared by electrodeposition were characterized by increased surface roughness.[68]

Several metallurgically prepared Ni/Ti alloys have been studied.[69] They were characterized by η_{100} between 425 and 600 mV (1 M NaOH, 25 °C). The electrocatalytic activity decreases in the order: $TiNi_2$ > $TiNi_3$ > $TiNi_4$ > Ti_2Ni > TiNi > Ti_3Ni > $TiNi_{0.7}$.

Hydrogen-absorbing alloys of $LaNi_5$ type are also very active for hydrogen evolution.[70–72] Microencapsulation of these powders in copper increases their mechanical stability during prolonged HER.[71]

Composite electrodes consisting of hydrogen-absorbing Ti_2N, $LaNi_5$ or mischmetal based alloy powders and electrodeposited Ni/Mo[73–75] were found to be very active, with overpotentials $\eta_{200} < 90\,\text{mV}$. As these alloys can absorb hydrogen, the electrodes obtained are more resistant to power interruptions because their potential stays negative at the open circuit. Coating containing binary Ni and TiH catalysts[76] were also found to be very active and immune to current interruptions.

Table 3. Activities of alloys and composite materials towards the HER.

Electrode	Conditions	b (mV dec^{-1})	Activity	Ref.
Mild steel	28% KOH, 75 °C	130 low c.d.; 115 high c.d.	$\eta_{135} = 406$ mV	[53]
Ni/Fe (40/60%); electrodeposited	28% KOH, 80 °C	72 low c.d.; 108 high c.d.	$\eta_{135} = 162$ mV	[53]
Ni/Mo (30/70 at%)	30% KOH, 70 °C		$\eta_{1000} = 83$ mV	[54]
Ni/Mo (75/25%); thermally activated	6 M KOH, 80 °C	112 low c.d.; 105 high c.d.	$\eta_{300} = 147$ mV to 185 mV after 1000 h operation	[56]
$Ni_{60}Mo_{40}$ ball milled	30% KOH, 70 °C	50	$j_0 = 17$ mA cm^{-2}; $\eta_{250} = 58$ mV	[58]
$Ni_{60}Mo_{40}$ arc melted	30% KOH, 70 °C	107	$j_0 = 42$ μA cm^{-2}; $\eta_{250} = 404$ mV	[58]
NiMo	1 M NaOH, 25 °C	132	$j_0 = 79$ μA cm^{-2}	[60]
Ni_2Mo	1 M NaOH, 25 °C	142	$j_0 = 70$ μA cm^{-2}	[60]
Ni_3Mo	1 M NaOH, 25 °C	148	$j_0 = 32$ μA cm^{-2}	[60]
NiMo(66.2/33.8%)	30% KOH, 25 °C	185	$j_0 = 2.8$ mA cm^{-2}; $\eta_{100} = 262$ mV	[275]
$Ni_{79}Mo_{20}Cd_1$	1 M NaOH	30–38 low c.d.; 120–125 high c.d.	$\eta_{100} \sim 140$ mV; at 68 °C	[62]
Ni/Mo/Fe	6 M KOH	115 low c.d.; 165 high c.d.	$\eta_{300} = 187$ mV	[64]
Ni/Mo/Cu	6 M KOH	28 low c.d.; 180 high c.d.	$\eta_{300} = 190$ mV	[64]
$Ni_{150}Mn_{50}Fe_{10}$	30% KOH, 30 °C	235	$j_0 = 40$ mA cm^{-2}; $\eta_{250} = 190$ mV	[67]
Co particles in electrodeposited Ni	5 M KOH, 25 °C	90	$\eta_{100} = 290$ mV	[84]
Fe particles in electrodeposited Ni	5 M KOH, 25 °C	78	$\eta_{100} = 250$ mV	[84]
Ni/V (75/25 at%)	30% KOH, 70 °C		$\eta_{1000} = 120$ mV	[54]
Co/Mo (80/20 at%)	30% KOH, 70 °C		$\eta_{1000} = 120$ mV	[54]
Ni/W (73/27 at%)	30% KOH, 70 °C		$\eta_{1000} = 134$ mV	[54]
Fe/Mo (54/46 at%)	30% KOH, 70 °C		$\eta_{1000} = 181$ mV	[54]
$Ni_{70}Mo_{15}Fe_{15}$	6 M KOH, 80 °C	120 low c.d.; 110 high c.d.	$\eta_{300} = 149$ mV to 187 mV after 1000 h operation	[56]
$LaPO_4$ bonded Ni powder	1 M KOH, 25 °C	130	$j_0 = 3.8$ mA cm^{-2}; $\eta_{250} = 236$ mV	[77]
$LaPO_4$ bonded Ni powder	9 M KOH, 70 °C	144	$j_0 = 6.3$ mA cm^{-2}; $\eta_{250} = 230$ mV	[276]
$LaPO_4$ bonded Ru (1%) on Ni	1 M KOH, 25 °C	64	$j_0 = 54$ mA cm^{-2}; $\eta_{250} = 42$ mV	[79]
$LaPO_4$ bonded Rh (3.5%) on Ni	1 M KOH, 25 °C	77	$j_0 = 27$ mA cm^{-2}; $\eta_{250} = 74$ mV	[79]
$LaPO_4$ bonded graphite	1 M KOH, 25 °C	133	$\eta_{250} = 525$ mV	[85]
$LaPO_4$ bonded Rh (0.1 at%)/C	1 M KOH, 25 °C	187	$\eta_{250} = 137$ mV	[85]
$LaPO_4$ bonded Pt (0.06 at%)/C	1 M KOH, 25 °C	95	$\eta_{250} = 103$ mV	[85]
$LaPO_4$ bonded Ru (0.1 at%)/C	1 M KOH, 25 °C	49	$\eta_{250} = 58$ mV	[85]
Ni/Mo (30/70%) pressed powders	1 M NaOH, 25 °C	140	$\eta_{250} = 177$ mV	[88]
Ni/Sn (50/50%)	11 M NaOH, 90 °C	50	$\eta_{300} = 100$ mV	[66]
Ti_2Ni + Ni/Mo	30% KOH, 70 °C		$\eta_{200} = 60$ mV	[73]
Ni + $PW_{12}O_{40}^{4-}$	1 M H_2SO_4, 25 °C	180	$\eta_{100} = 180$ mV	[90, 91]
Ni + Cu + $Pmo_{12}O_{30}^{3-}$	1 M H_2SO_4, 25 °C	260	$\eta_{250} = 160$ mV	[96]

3.3 Composite coatings

Several composite coatings have been used to increase the electrocatalytic activity for the HER. For example, Ni[77, 78] powder has been bonded with inorganic polymer $LaPO_4$ prepared in situ (Table 3). The electrochemical surface roughness factor is 5000 and few percent of the polymer makes the material rigid and stable in alkaline solutions.[78] Chemical deposition of Ru[79] or Rh[80] on Ni powder followed by bonding with $LaPO_4$ produces extremely active materials with η_{250} of 40–60 mV.

Electrodeposition of Ni in the presence of PTFE (Teflon) fine (0.2 μm) particles reduces μ_{10} by 228 mV.[81] Other PTFE-bonded electrodes were prepared by mixing active powders with PTFE suspension followed by sintering.[82, 83] Comprehensive study of various PTFE bonded materials have revealed no important gain in activity of such materials.[83] PTFE bonded powders are widely used in fuel cells.

Incorporation of Ni, Co and Fe particles into the electrodes during Ni plating (composite coating) increases activity for HER by over 200 mV in comparison with the nickel electrode.[84] The materials obtained are more porous, with surface roughness factors up to 200.

Graphite particles containing Pd, Pt or Rh (0.1 at%) were deposited with nickel from the Ni plating bath or bonded with $LaPO_4$.[85, 86] $LaPO_4$ bonded materials have shown a significant decrease in the hydrogen overpotential. Sputtering Pt on HOPG does not produce stable materials.[87]

Pressing Ni and Mo powders together significantly decreases hydrogen overpotential.[88] Introduction of oxygen to Ni/Mo alloys using arc ion plating process decreases hydrogen overpotential.[89] Overpotential $\eta_{400} = 90$ mV (32.5% NaOH, 90 °C) was reported for 6 at% of oxygen. Further addition of oxygen deactivates the electrode as nickel oxides are formed.

Deposition of metals [Ni,[90–94] Co,[95] Ni/Cu,[96] Fe,[94] Pd,[97, 98] Pt/Co[99]] with heteropolyacids [$PW_{12}O_{40}$,[3, 90–96] $PMo_{12}O_{40}$,[3, 94, 96] $SiW_{12}O_{40}$[4, 91, 95, 97–99]] increases activity for the HER in alkaline[92–95, 98, 99] and acid[90, 91, 93, 96, 97] solutions. The Tafel curves are characterized by one or two slopes and the estimated surface roughness of Ni/$PW_{12}O_{40}$ deposits is ~50, which indicates a real electrocatalytic effect (Table 3).

4 HYDROGEN EVOLUTION ON RANEY TYPE MATERIALS

Raney-type materials are alloys of electrocatalytically active metals (Ni, Co, Cu) with active metals as Al or Zn. Active metals may be easily leached out in alkaline solution (usually in 30% KOH, 70 °C), leaving a very porous structure. The main purpose of using Raney alloys is to increase the real surface area, although surfaces of very rough structures may also have higher electrocatalytic activity.

The oldest known Raney alloy is Raney nickel,[100–103] which is an alloy of 50/50% wt of Ni and Al. Initially applied to catalytic hydrogenation of organic compounds it also found applications as an electrocatalytic material for the HER. Subsequently, Raney Ni was modified with various elements and other metals were used for its preparation (Raney Cu,[104] Devarda Cu,[104] Raney Co,[105] etc.).

4.1 Raney Ni/Al

The original Raney Ni composition, 50/50% wt Ni/Al corresponds to 31.5/68.5 at%, respectively. Completely leaching aluminum from this alloy leaves a very porous material with ~77% porosity and very large real surface area of over 100 $m^2\ g^{-1}$.[106] The real surface area of Raney Ni powders depends on the conditions of leaching aluminum (concentration of alkaline solution, temperature, time,[106] surface oxidation[107], addition of complexing agents, etc.). The kinetics of the leaching process has also been studied.[108–110] Alloying of Ni and Al leads to the formation of various phases: $NiAl_3$, Ni_2Al_3, NiAl, Ni_3Al, etc. (see Ref. [6], p. 40). Each phase is characterized by a different kinetics of decomposition in alkaline solution and the rate of leaching of Al decreases in the order: $NiAl_3 > Ni_2Al_3 > NiAl$. The residual aluminum plays an important role in the electrodes activity and to obtain the highest activity 5–6 wt% of Al should be left in the electrode after leaching.[111]

The original Raney Ni is a powder and it is not well suited for water electrolysis, although its activity in such a form has been studied.[112] Practical electrodes are prepared by:

- electrocodeposition (composite coating) of Raney Ni powder with Ni (powder was suspended in Ni plating bath),[105, 113–115] A special device allowing a uniform deposition was also developed;[105, 114]
- plasma[116–119] or wire-arc[120] spraying;
- cold rolling of Al foil on Ni followed by annealing at 730 °C;[121]
- rolling of Raney Ni and Ni powder on Ni plates followed by a heat treatment at <700 °C;[117, 122]
- interdiffusion of Al into Ni above the Al melting point by Ni aluminization using flame spraying, dipping into molten Al[123] or heating a mixture of Ni and Al powders;[124]
- pressing and sintering Raney Ni with carbonyl nickel powder leading to a porous material (DSK Raney nickel);[102, 125]

- sintering of Raney Ni at 1400 °C under high pressure (1000 atm) in argon atmosphere[127] or alloying it with nickel;[128]
- pressing Raney Ni and Ni powders,[127] etc.

The electrodes obtained belong to the most active electrode materials, with overpotentials η_{250} often below 100 mV. However, there is a problem with the long-term physical stability and activity of these materials; during prolonged electrolysis they become brittle and tend to disintegrate, although their activity may increase.[121]

After leaching Al, the electrode structure becomes amorphous or nanocrystalline.[127] The crystallite size of plasma-sprayed Raney Ni/Al was estimated as 6.5 nm and that of Raney Ni/Al/Mo as 3.5 nm.[129] The leached materials are pyrophorous and must not be exposed to air. It is usually necessary to oxidize their surface to stabilize them. Results obtained for various electrodes are shown in Table 4. Electrodes prepared by sintering Raney Ni were characterized by large Tafel slopes (275 mV dec^{-1}) and $\eta_{250} = 116$ mV in 1 M NaOH at 70 °C. This behavior indicates influence of porosity, which may double Tafel slopes. Pressing Raney Ni and Ni powders (50% wt) increases their activity ($b = 62$ mV dec^{-1}, $\eta_{250} = 56$ mV in 1 M NaOH, 70 °C). Very active electrodes are also prepared by interdiffusion of Al into Ni above the Al melting point.[124] An increase in the concentration of hydroxide usually decreases the electrocatalytic activity, while an increase in temperature increases the activity. It is interesting to note that these porous electrodes have intermediate slopes, between 40 and 120 mV dec^{-1} predicted for the Volmer–Heyrovsky reaction mechanism. A.c. impedance studies display porous electrode behavior.[128]

Tanaka *et al.*[130] have studied activity of the precursor phases $NiAl_3$, Ni_2Al_3, NiAl and Ni_3Al. The most active phase is $NiAl_3$, followed by Ni_2Al_3, the others are not much more active than Ni, because Al could not be leached out from these materials. The estimated surface roughness was 1.3×10^4 and 9.3×10^3 for $NiAl_3$ and Ni_2Al_3, respectively. These values are much smaller than those obtained for more deeply leached Raney Ni electrodes, where roughness factors of $4.5–6 \times 10^4$ were obtained.[119, 124] Conflicting results were reported on the influence of the electrochemical oxidation of the surface after leaching: some authors found a decrease of activity and an increase of the Tafel slope for pure Raney Ni(Al) electrodes[124, 127] while others marked increased activity and decrease of the Tafel plots from 110 to 60–70 mV dec^{-1} for composite coated Raney Ni electrodes.[130] This effect may be connected with different oxidation potentials used in both experiments. Too strong oxidation usually reduces the electrode activity. It has been also reported that this activation by oxidation is temporary as even β-$Ni(OH)_2$ is reduced during long-term hydrogen evolution.[131]

Table 4. Activities of Raney Ni/Al based electrodes towards the HER.

Electrode	Conditions	b (mV dec^{-1})	Activity	Ref.
Sintered Raney Ni	1 M NaOH, 70 °C	275	$\eta_{250} = 116$ mV	[126]
Raney Ni and Ni pressed powders	1 M NaOH, 70 °C	62	$\eta_{250} = 56$ mV	[127]
Heated Ni and Al powders	1 M NaOH, 70 °C	40	$\eta_{250} = 53$ mV	[124]
Electrocodeposited Raney Ni with Ni	1 M NaOH, 70 °C	57–76	$\eta_{250} = 59$ mV	[277]
Plasma sprayed Raney Ni	25% KOH, 70 °C	84	$\eta_{250} = 119$ mV	[119]
Plasma sprayed Raney Ni/Mo	25% KOH, 70 °C	51	$\eta_{250} = 74$ mV	[119]
$NiAl_3$	1 M NaOH, 30 °C	Nonlinear	0.186	[129]
Ni_2Al_3	1 M NaOH, 30 °C	Nonlinear	0.316	[129]
Raney Ni powder	6 M KOH, 23 °C		$\eta_{100} = 0.3$ A g^{-1}	[132]
Raney Ni + 4% Ti			$\eta_{100} = 0.48$ A g^{-1}	[132]
Raney Ni + TiH_2 (10%)	1 M NaOH, 30 °C	118	$\eta_{250} = 118$ mV	[136]
Raney Ni + 8.9% Fe			$\eta_{100} = 1.2$ A g^{-1}	[132]
Raney Ni + 7.5% Mo			$\eta_{100} = 4.6$ A g^{-1}	[132]
Raney Ni + 0.4% Cr	6 M KOH, 60 °C		Decrease of η_{250} by ~43 mV	[134]
Plasma sprayed Raney Ni + Mo	25% KOH, 70 °C		$\eta_{1000} = 70–90$ mV	[118]

There have been many attempts to improve Raney Ni based materials by doping them with other metals. Doping increases the activity and stability of the materials although several simple Raney Ni electrodes were not optimized. Attempts were made to dope Raney Ni/Al alloys with Fe,[132] Ti,[132–136] Mo,[132] Cr,[134, 135] Sn,[137] Cr/Co, Cr/Mo and Cr/Ti,[138] etc. In each case, the decrease of the overpotential was observed (see Table 4). Addition of molybdenum to plasma sprayed electrodes seems to be the most promising.[118, 119] It has been suggested that a ternary phase Mo_2NiAl_5 may be responsible for the high activity,[139] however, this pure phase disintegrates during leaching in alkaline solutions and cannot be studied.[140] A comparison of activities of polycrystalline Ni and Raney Ni electrodes is displayed in Figure 3. The current on Ni/Al/Mo electrode is over 1000 times larger than that on polycrystalline Ni.

To improve the electrode's long term stability and immunity to current interruptions the addition of nickel-based metal hydride to composite coated Raney Ni has been proposed.[141]

4.2 Raney Ni/Zn

Another very active of Raney Ni materials are alloys of Ni with Zn. They are, in principle, similar to Ni/Al alloys, from which Zn may be easily leached out in alkaline solutions. They may be prepared by direct alloying of Ni and Zn,[142] sherderizing i.e., exposing nickel to zinc vapor at 390 °C under N_2 for 8 h,[143] but most often they were prepared by d.c. galvanic deposition.[144–146] Galvanostatic pulse and pulse reverse techniques are also employed.[147] Ni/Zn alloys exhibit an anomalous

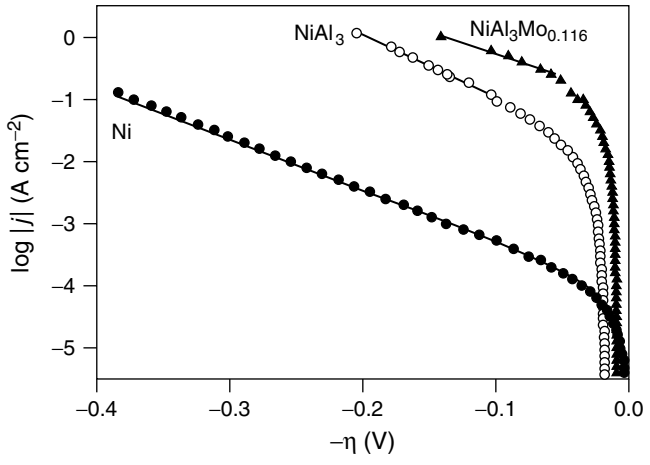

Figure 3. Stationary Tafel curves on polycrystalline Ni and two Raney type materials: Ni_2Al_3 and $NiAl_3Mo_{0.116}$ (after leaching out Al), obtained in 1 M KOH at 25 °C.[36, 140]

deposition in which the less noble metal i.e., Zn is preferentially deposited.[148] They form three major phases: α, γ and η; for a phase diagram see Ref. [149]. The α-phase is a solid solution of Zn in Ni and an equilibrium solubility is about 30%, the γ-phase corresponds to the composition Ni_5Zn_{21} and the η-phase is a solid solution of Ni in Zn with Ni solubility less than 1%. Other phases (β : NiZn and δ : Ni_3Zn_{22}) have not been obtained by galvanic deposition.[144] By changing deposition potential the alloy composition may be easily changed between 24 and 70 wt% of Ni.[150]

Leaching Zn produces a "dry mud" type structure, containing cracks and pores.[143, 150] The structure of the deposit after leaching is amorphous or microcrystalline.[53, 151] Zinc cannot be totally leached out from these alloys in alkaline solutions.[149] The activity of the leached Ni/Zn alloys depends strongly on the precursor alloy composition, increasing with the decrease in Ni content in the precursor alloy[150] (see Table 5). Such an increase in apparent activity was attributed to the increase in the real surface area, the surface roughness increases from 100 to 1000 with a decrease in the Ni content from 70 to 28%.[150]

Activity of Ni/Zn electrodes depends on the thickness of the deposited layer, increasing with the increase in the layer thickness (Table 5).[143] The slope of dη/d log d equals 60 to 80 mV dec^{-1} at current densities of 0.1 and 1 A cm^{-2}, respectively. An increase in layer thickness increases the real surface area of the electrode. The electrode activity is maintained after prolonged electrolysis.[152]

Improvement in electrodeposition of Raney Ni alloys has been obtained by a slow addition of $ZnCl_2$ to the plating bath.[153, 154] Materials deposited in such a way contained composition gradient, with higher Zn content closer to the outer surface. Such electrodes are characterized by a large surface roughness of 2200 and better adherence.[154]

4.3 Other Raney Ni based materials

Ni/Co/Zn electrodes are characterized by activity similar to Ni/Zn materials, although the surface roughness of the former is larger.[151] An example of Tafel plots obtained on these electrodes is presented in Figure 4. Further improvements have been obtained using zinc gradient in the deposit, as described above. Such electrodes had roughness factor of 4400 and slightly higher activity, $\eta_{135} = 90$ mV.[154] They are characterized by low Tafel slopes of 53 mV dec^{-1} at 65 °C.[153]

Ni/Fe/Zn electrodeposited alloys are new promising electrodes for hydrogen evolution.[155] They show good activity and stability at prolonged polarizations. Their advantage

Table 5. Activities of Raney Ni/Zn based electrodes towards the HER.

Precursor alloy	Conditions	b (mV dec^{-1})	Activity	Ref.
Ni(28%)/Zn	1 M NaOH, 25 °C	69	$\eta_{250} = 206$ mV	[150]
Ni(38%)/Zn	1 M NaOH, 25 °C	75	$\eta_{250} = 263$ V	[150]
Ni(61%)/Zn	1 M NaOH, 25 °C	76	$\eta_{250} = 301$ mV	[150]
Ni(70%)/Zn	1 M NaOH, 25 °C	90	$\eta_{250} = 402$ mV	[150]
Ni(54%)/Zn	28% KOH, 70 °C	62	$\eta_{135} = 115$ mV	[150]
Ni_5Zn_{21}, 12 μm	40% KOH, 115 °C		$\eta_{100} = 174$ mV	[143]
Ni_5Zn_{21}, 300 μm	40% KOH, 115 °C	75	$\eta_{100} = 23$ mV	[143]
Ni_5Zn_{21}, 300 μm	40% KOH, 115 °C	75	$\eta_{1000} = 56$ mV	[143]
Ni/Zn with a composition gradient	6 M KOH, 70 °C	81	$\eta_{135} = 100$ mV	[153, 154]
Ni/Co/Zn with a composition gradient	6 M KOH, 70 °C	53 at 65 °C	$\eta_{135} = 90$ mV	[154]
Ni/Fe/Zn	1 M NaOH, 80 °C	67	$\eta_{135} = 104$ mV	[155]
Ni/Fe/Zn	28% KOH, 80 °C		$\eta_{135} = 100$ mV	[155]
Ni/P/Zn	30% KOH, 70 °C	47	$\eta_{250} = 157$ mV	[156]

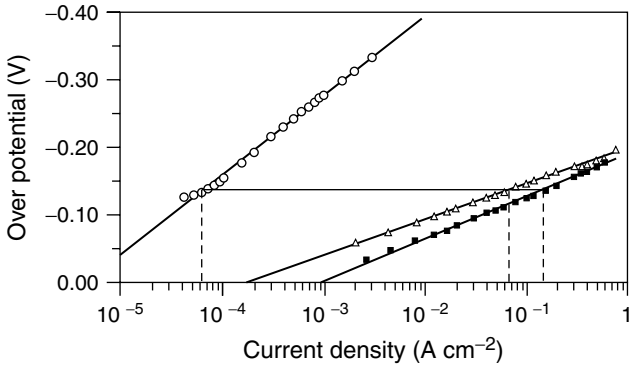

Figure 4. Tafel plots obtained in 0.5 M NaOH on: (○) polished Ni; (△) Ni/Zn and (●) Ni/Co/Zn alloys, after leaching out Zn.[151]

may also lie in their immunity to poisoning by residual iron always present in the electrolytic cell.

The most active Raney Ni/Zn precursor alloys containing large amount Zn are not very stable during prolonged electrolysis. Improvement has been obtained by deposition of Ni/P/Zn alloys.[156, 157] They were obtained by direct electrodeposition and deposition with the concentration gradient[156] and show very good stability and activity (see Table 5). A proprietary (Electrolyser Inc.) Raney type alloy is characterized by two low Tafel slopes (22 and 50 mV dec^{-1} at 79 °C) and low hydrogen overpotential.[158]

4.4 Reaction mechanism

Raney-based electrode materials are very porous. For porous electrodes in the absence of mass transfer limitations, a doubling of the Tafel slope is predicted theoretically.[159, 160] However, low Tafel slopes are usually observed on such electrodes (see Tables 4 and 5). Such slopes cannot be explained in terms of Volmer–Heyrovsky–Tafel reaction mechanism. It has been suggested[143] that such a behavior arises from the hydrogen pressure buildup (up to 80 MPa) in very narrow pores ($r \sim 10^{-7}$ cm). However, more rigorous calculations[161] show that even for the narrowest pores, low Tafel slopes could be observed at very low overpotentials only while, experimentally, the range of low slopes extends for hundreds of millivolts. It has been suggested, that such a small slopes may be caused by surface heterogeneity, that is distribution of hydrogen adsorption energies on different parts of the electrode, leading to the distribution of the rate constants.[162]

5 HYDROGEN EVOLUTION ON OXIDES, CARBIDES, SULFIDES, PHOSPHIDES, BORIDES AND SILICIDES

Oxides are mainly used for the oxygen evolution reaction (OER), however, some of them are also active for the HER.[162] Sulfides are active materials used for water electrolysis. Several materials described in this chapter are amorphous. For other amorphous materials, see Section 6.

5.1 Nickel oxide

Oxidation of nickel surface results in increased activity towards the HER in alkaline solutions. Electrochemical

oxidation of Ni changes the reaction mechanism from one slope of 115 mV dec^{-1} to two slopes: 75 mV dec^{-1} at lower and 269 mV dec^{-1} at higher overpotentials[35] (see Table 6). At $\eta = -0.3$ V there is about tenfold increase in the HER current after oxidation. Its activity increases with increase of the oxidation potential up to 0.4 V versus Hg/HgO reference electrode, which corresponds to the formation of $Ni(OH)_2$.[163] At more positive potentials, deactivation of the electrode is observed. This oxide may be reduced at more negative potentials (−1.8 V versus Hg/HgO) and the electrolysis should be carried out at potentials not exceeding −1.3 V.

5.2 RuO_2 and IrO_2

Ruthenium and iridium oxides were initially developed for the dimensionally stable anodes (DSA) in chlor-alkali industry.[7, 164] They are usually obtained by: thermal decomposition of appropriate precursors dissolved in suitable solvents and spread on the metallic support, usually on Ti,[165] reactive sputtering,[166] sintering of colloidal particles,[167] electrocodeposition of the particles from the Ni Watts bath,[168–170] etc. These oxides can be used in alkaline and acidic solutions. Nonstoichiometric and porous layers are usually obtained and their properties depend on the procedure used and temperature of calcinations. Samples obtained by thermal decomposition display a cracked-mud structure.[171]

Initially formed layers exhibit an activation phenomenon, the electrode activity towards the HER increases over 10 times when the applied potential was in the HER region during 2–3 h.[172] The immersion of the electrode in solution is not sufficient to activate the electrode. The activation phenomenon does not cause any modification of the chemical state of Ru atoms at the electrode surface (no reduction of RuO_2). The electrode is deactivated after its removal from solution. It has been suggested that H chemisorption within the structure is responsible for this process. This activation process increases the surface roughness of thin RuO_2 layers by 20–30%.[173] The capacitance of these oxides is very large, up to 1 F cm^{-2}.[169]

The surface state of the oxides has often been studied by measurement of the voltammetric surface charge. On monocrystalline RuO_2 distinct voltammetric peaks appear, attributed to H adsorption on the crystal surface.[174] On polycrystalline samples distinct peaks are not observed.[7, 175] Recent in situ surface enhanced Raman scattering studies suggest reduction of RuO_2, probably to Ru^{3+} oxides/hydroxides.[176] Usually two Tafel slopes are observed, 40–60 mV dec^{-1} at low overpotentials and a higher 120–240 mV dec^{-1}. Iridium oxides are more active than RuO_2 and their mixtures are often used. Several experimental results are displayed in Table 6.

5.3 Reaction mechanism

Hydrogen evolution mechanism on oxides is different from that on metallic electrodes. It has been suggested that it proceeds through the reduction of oxide on the electrode surface in acidic:[177]

$$\text{M–OH} + \text{H}^+ + \text{e} \rightleftharpoons \text{M–OH}_2 \quad (26)$$

$$\text{M–OH}_2 + \text{H}^+ + \text{e} \rightleftharpoons \text{M–OH} + \text{H}_2 \quad (27)$$

or in alkaline solutions

$$\text{M–OH} + \text{H}_2\text{O} + \text{e} \rightleftharpoons \text{M–OH}_2 + \text{OH}^- \quad (28)$$

$$\text{M–OH}_2 + \text{H}_2\text{O} + \text{e} \rightleftharpoons \text{M–OH} + \text{H}_2 + \text{OH}^- \quad (29)$$

An alternative mechanism, involving formation of a direct M–H bond, has also been proposed[162] in which reaction (26) is followed by

$$\text{M–OH}_2 + \text{e} \rightleftharpoons \text{M–H} + \text{OH}^- \quad (30)$$

$$\text{M–H} + \text{H}_2\text{O} \longrightarrow \text{M–OH} + \text{H}_2 \quad (31)$$

The reaction mechanism has been studied in detail for $RuO_2 + IrO_2$ electrodes. These are nonstoichiometric materials and their activity depends on the temperature of decomposition of corresponding precursors. Reaction order in acidic solutions at a constant overpotential is zero independently of oxide composition.[178] The apparent reaction order at a constant potential changes monotonically from 2.5 for pure IrO_2 to one for pure RuO_2. Tafel slopes change from ~25 mV dec^{-1} for IrO_2 to 60 mV dec^{-1} for pure RuO_2, with the slope of 40 mV dec^{-1} for 70% RuO_2. Tafel slope of 240 mV dec^{-1} was also reported at higher overpotentials.[179] In alkaline solutions IrO_2 electrodes are characterized by two Tafel slopes: 40 mV dec^{-1} at low overpotentials and 120 mV dec^{-1} at higher overpotentials.[183] The reaction order at a constant potential, with respect to OH^-, is ~ -0.5 at low overpotentials. Assuming transfer coefficient of 0.5 this leads to the chemically significant reaction order $\beta_{OH^-} = -1$.

5.4 Other oxides

Spinel structured Co_3O_4, which is usually used for the OER, may also be used for the HER in alkaline solutions.[181] Pure compound displays strange behavior; two Tafel slopes

Table 6. Activities of oxide electrodes towards the HER.

Electrode	Conditions	b ($mV\,dec^{-1}$)	Activity	Ref.
Polished Ni	1 M NaOH, 25 °C	115	$\eta_{250} = 530\,mV$	[35]
Electrochemically oxidized Ni	1 M NaOH, 25 °C	75 low η; 269 high η	$\eta_{250} = 320\,mV$	[35]
RuO_2	1 M H_2SO_4, 25 °C	40 at low η; 240 at high η	$\eta_{100} = 250\,mV$	[179]
RuO_2, thin layer	1 M NaOH, 25 °C	40–50 low η; 230–240 high η		[278]
RuO_2	1 M NaOH, 20 °C	37 low η; 70 high η	$\eta_{100} = 115\,mV$	[279]
RuO_2	1 M NaOH, 25 °C	60	$\eta_{250} = 96\,mV$	[169]
RuO_2	1 M NaOH, 70 °C	40	$\eta_{250} = 86\,mV$	[169]
IrO_2	1 M NaOH	40 at low η; 120 at high η		[180]
IrO_2	1 M $HClO_4$	35–50 depending on the calcination T	$\eta_{1000} = 100\,mV$	[280]
IrO_2	1 M H_2SO_4, 25 °C	40 at low η; 240 at high η	$\eta_{100} = 127\,mV$	[179]
IrO_2/RuO_2	1 M $HClO_4$	20–60 mV 0 to 100% RuO_2	$\eta_{100} = 140$ to 250 mV	[178]
Ti/Co_3O_4; $Ti/RuO_2/Co_3O_4$	1 M NaOH, 25 °C	60 mV; 40 mV		[181]
$LaNiO_3$/Ni	3 M KOH, 25 °C		$\eta_{250} = 320\,mV$	[182]

have been observed: $180\,mV\,dec^{-1}$ at low overpotentials followed by $60\,mV\,dec^{-1}$ at high overpotentials. On the other hand the electrode prepared with undercoating of RuO_2 showed slopes of $40–120\,mV\,dec^{-1}$, the latter electrode being much more active than the former. The apparent activities are larger for $Ti/RuO_2/Co_3O_4$ than Ti/Co_3O_4. The reaction orders versus OH^- are -1 and -0.5 for these electrodes, respectively.

Lanthanum nickelate, $LaNiO_3$, obtained by calcinations of the corresponding salts and electrocodeposited with Ni shows increased activity towards the HER.[182] It is more active than the sintered Ni, with $\eta_{250} = \sim 0.32\,V$.

5.5 Sulfur containing alloys

Sulfide coating may be easily obtained by electrodeposition of Ni from the baths containing thiourea,[183, 184] SCN^-,[185] $S_2O_3^{2-}$,[186, 187] suspended particles of the corresponding sulfides,[186] and gas phase reactions between Ni and S or H_2S.[187] The sulfide most often studied is NiS_x. It was obtained in compositions containing 4.2%S,[185] 10–20%S,[186] Ni_3S_2, α-Ni_7S_6 and α-Ni/S.[187] It has been reported that during cathodic HER, sulfur is leached out from the deposit.[185, 187] After 3000 h of electrolysis all nickel sulfide had disappeared from the XRD spectra, leaving porous Raney Ni coatings containing ~3% of S.[187] Properly prepared electrodes are very active. Comparison of the activities of various sulfides is displayed in Table 7. Some deactivation with time was observed.[187]

The addition of fine powders containing metal sulfides affects the electrode activity. Conflicting results have been reported on the influence of the incorporated NiS powder in Ni.[176] Addition of various forms of NiS powders decreases activity of NiS_x deposit while addition of MoS_2 improves the activity.[186, 189] Amorphous FeS_x films corrode even during hydrogen evolution.[190] Another very active sulfide, $NiCo_2S_4$, has been operated for several thousands hours at $1\,A\,cm^{-2}$ with the overpotential of 100 mV.[191, 192] $Mo_2Ru_2Se_8$ clusters also show high activity.[193]

Electrodes containing incorporated sulfide powders become immune to the contamination of the electrolytic solution by Fe.[186] However, metal sulfide coated metallic parts cannot be welded or heat-treated as they become very brittle.[6]

5.6 Phosphorous-containing alloys

MeP_x alloys may be easily obtained by electrodeposition from solutions containing H_3PO_3,[194–196] $H_2PO_2^-$,[194, 197] by electroless deposition[198] or fast quenching.[199] These materials are often used for corrosion protection. The system most studied was Ni/P. Mechanism of deposition has been studied in several papers.[196–203] Deposited materials may be either amorphous or crystalline. It has been

Table 7. Activities of sulfides towards HER.

Electrode	Conditions	b (mV dec^{-1})	Activity (mV)	Ref.
Ni (82.4%) S (10.5%)	1 M KOH, 25 °C	118	$\eta_{10} = 160$[a]	[184]
Ni/S freshly deposited	40% KOH, 22 °C	70–80	$\eta_{100} = 210–150$	[187]
Ni/S, aged 3000 h	40% KOH, 117 °C	30	$\eta_{1000} = 105$	[187]
Ni/S (4.2%)	28% KOH, 23 °C; 28% KOH, 80 °C	85, 47 low, 73 high currents	$\eta_{135} = 289$; $\eta_{135} = 189$	[185]
Ni + MoS_2	6 M KOH, 25 °C	50 to 200 nonlinear	$\eta_{100} = \sim 150$	[189]
Ni + NiFeS	6 M KOH, 25 °C; 6 M KOH, 80 °C	62, 105, 45 low, 65 high currents	$\eta_{135} = 219$; $\eta_{135} = 128$	[188]

[a]With respect to the real surface area obtained by BET.

suggested[204] that alloys with low P content are crystalline, at 10–15 at% of P transition is observed from amorphous to crystalline state, and for higher P content the samples amorphous. Others reported that the alloys containing less than 14 at% of P were crystalline.[205] Nevertheless, other authors[195, 208] have found that alloys containing 6–8% of P are amorphous and become crystalline after heat treatment at 400 °C. Crystallization leads to a formation of Ni_3P and Ni crystals. Amorphous alloys contain small amount of nanocrystals of Ni and Ni_3P floating in the amorphous phase.[206] Presence of crystallites of Ni_5P_2 has also been observed.[207]

Activities of Ni/P alloys are presented in Table 8. They depend on the phosphorous content and, in general, decrease with increase in P content.[195, 198, 208] Burchardt *et al.*[206] have found that for amorphous materials,

Table 8. Activities of MeP_x alloys for the HER.

Electrode	Conditions	b (mV dec^{-1})	Activity	Ref.
NiP (3 wt%, ~5.5 at%)	1 M KOH, room T	57	$\eta_{250} = 200$ mV	[208]
NiP (10 wt%, ~18 at%)	1 M KOH, room T	112	$\eta_{250} = 520$ mV	[208]
$Ni_{70}P_{30}$	0.5 M KOH, 25 °C	115	$\eta_{135} = 1239$ mV	[53, 281]
$Ni_{70}P_{30}$	1 M NaOH, 70 °C	136 low currents; 244 high currents	$\eta_{250} = 698$ mV	[195]
$Ni_{73}P_{27}$	1 M NaOH, 70 °C	109	$\eta_{250} = 358$ mV	[195]
$Ni_{92}P_8$	1 M NaOH, 70 °C	57	$\eta_{250} = 171$ mV	[195]
$Ni_{92}P_8$, heated 4 h at 400 °C	1 M NaOH, 70 °C	120	$\eta_{250} = 330$ mV	[195]
$Ni_{93}P_7$ (3.8 wt%) optimized	1 M NaOH, 25 °C		$j_{150} = 159$ mA cm^{-2}[a]	[197]
$Ni_{87.5}P_{12.5}$, crystal size 10–20 nm; $Ni_{89}P_{11}$, 5–10 nm; $Ni_{83}P_{17}$ < 5 nm	1 M NaOH, 25 °C		$j_{(E=-1.18\ V\ SCE)}$; 90 mA cm^{-2}; 0.25 mA cm^{-2}; 0.07 mA cm^{-2}	[206]
$Co_{72}P_{28}$	0.5 M KOH, 25 °C	57	$\eta_{135} = 535$ mV	[53, 281]
Co/P (1 wt%)	1 M KOH, 20 °C	50	$j_{200} = 175$ mA cm^{-2}	[209]
$Ni_{40}Co_{23}P_{27}$	0.5 M KOH, 25 °C	57	$\eta_{135} = 637$ mV	[53, 281]
$Ni_{72}Fe_1P_{27}$	0.5 M KOH, 25 °C	22 low currents; 42 high currents	$\eta_{135} = 312$ mV	[53, 281]
Ni/Fe/P (9.5, 86, 3 wt%)	1 M KOH, 25 °C	70–90	$j_{200} = 7.9$ mA cm^{-2}	[209]

[a]Current density at $\eta = 150$ mV.

electrocatalytic activity increases with the decrease in size of Ni crystals and disappearance of Ni_3P, Table 8. There are conflicting reports on the influence of various activation techniques on the electrode activity. Podesta *et al.*[198] found that heat treatment, electrochemical oxidation and treatment in 7 M HNO_3 of electroless Me/P alloys improve their activities. Others found that heat treatment[195, 208] or anodic oxidation[195] lead to deactivation of electrodes. On active electrodes low Tafel slopes ($\sim$57 mV dec^{-1}) have been found. On less active electrodes an increase in Tafel slope at higher overpotentials was observed. Several authors suggested that Ni/P alloys may absorb important amounts of hydrogen.[206, 208–211] Paseka[208, 209] has determined electrode capacitances (30–50 mF cm^{-2}) from the slopes of open circuit potential relaxation curves and attributed them to the hydrogen absorption. Burchardt[211] has studied oxidation of Ni/P electrodes after hydrogen evolution and found that the current decreases proportionally to $t^{-1/2}$, which might indicate hydrogen oxidation from the bulk alloy. On the other hand ac impedance measurements displayed, on the complex plane plots, a simple semicircle or a straight line followed by a semicircle, characteristic for porous electrodes.[195] The estimated values of the double layer capacitance were 30–50 mF cm^{-2}. This result was attributed to a high surface roughness of 15–2500. Important dependence of the electrode activity on the thickness of the deposited layer was also observed.[211] Thin deposits are characterized by the Tafel slope of 120 mV dec^{-1} while thicker deposits display a low Tafel slope of $\sim$60 mV dec^{-1} at lower and $\sim$120 mV dec^{-1} at larger overpotentials. Such behavior may indicate Frumkin isotherm for hydrogen adsorption. Rough comparison of the kinetics of $Ni_{73}P_{27}$ and $Ni_{92}P_8$ electrodes suggests that, although the latter is characterized by much higher apparent activity, the intrinsic activities (per real surface area) of both electrodes are very similar[195, 212] (note errors in Tables 7 and 8 of Ref. [195]).

Alloys with other metals have also been studied. Co/P alloy containing 1 wt% of P is as active as Ni/P (3 wt%),[209] while that containing large amounts of P is inactive. Ni/Co/P and Ni/Fe/P are less active than other binary alloys. Long-term stability and activity of Ni/P alloys are good although they are sensitive to contamination by Fe.[209]

5.7 Borides

Ultrafine (20–100 nm) amorphous metal borides may be prepared by chemical reduction of metal salts with KBH_4.[213, 214] Nickel boride amorphous phases correspond roughly to Ni_2B. Because of a very large surface area it could be interesting for the alkaline HER. Activities of consolidated Ni_2B powders and their mixtures with nickel powder[40] are presented in Table 9. High electrocatalytic activities were attributed to a very large real surface area (roughness factor 1.2×10^4 and 5×10^4 for 100% and 90% nickel boride, respectively). This electrode was also active in electrocatalytic hydrogenation of organic compounds.[215, 216] Studies of several other Ni/B doped materials have revealed small increase in activity for certain metals (Co, Rh, Ru).[217]

5.8 Silicides

Silicides of several transition metals (Fe, Co, Ti, Ni, Zr, Cu, Cr, V, Ag, Mn, Pt, Pd) have been studied towards HER in alkaline[218] and acidic[219] solutions. The Tafel curves obtained were not linear and relatively high. These alloys were usually not very active except Pt/Si and Pd/Si and they often corroded in solutions.

5.9 Carbides

Tungsten carbide is a good material for hydrogen evolution in acidic media.[220] Graphite electrodes coated with α-WC

Table 9. Activities of amorphous nickel boride for the HER.

Electrode	Conditions	b (mV dec^{-1})	Activity (mV)	Ref.
Ni_2B	1 M NaOH, 70 °C	104	$\eta_{250} = 159$	[40]
Ni_2B, oxidized electrochemically	1 M NaOH, 70 °C	80	$\eta_{250} = 126$	[40]
Ni_2B + 10% Ni powder	1 M NaOH, 70 °C	57	$\eta_{250} = 113$	[40]
Ni/B	1 M NaOH, 70 °C	85	$\eta_{250} = 133$	[217]
Ni/B + 2% Co	1 M NaOH, 70 °C	68	$\eta_{250} = 100$	[217]
Ni/B + 2% Cr	1 M NaOH, 70 °C	81	$\eta_{250} = 112$	[217]
Ni/B + 2% Rh	1 M NaOH, 70 °C	69	$\eta_{250} = 96$	[217]
Ni/B + 2% Ru	1 M NaOH, 70 °C	72	$\eta_{250} = 94$	[217]

Table 10. Activities of amorphous alloys towards the HER.

Electrode	Conditions	b ($mV\,dec^{-1}$)	Activity	Ref.
$NiZr_2$ activated in 1 M HF	30% KOH, 70 °C	$107\,mV\,dec^{-1}$	$\eta_{100} = 298\,mV$	[225]
$NiZr_2$ amorphous powder, activated in 1 M HF	30% KOH, 70 °C	$165\,mV\,dec^{-1}$	$\eta_{250} = 296\,mV$	[227]
$NiZr_2$ activated in 1 M HF	30% KOH, 70 °C	$142\,mV\,dec^{-1}$	$\eta_{250} = 321\,mV$	[228]
$Ni_{0.4}Co_{0.6}Zr_2$ activated in 1 M HF, initial activity	30% KOH, 70 °C	$97\,mV\,dec^{-1}$	$\eta_{250} = 345\,mV$	[228]
$Ni_{0.4}Co_{0.6}Zr$ activated in 1 M HF, initial activity	30% KOH, 70 °C	$135\,mV\,dec^{-1}$	$\eta_{250} = 341\,mV$	[228]
$Fe_{60}Co_{20}Si_{10}B_{10}$	1 M KOH, 90 °C	$166\,mV\,dec^{-1}$	$\eta_{300} = 359\,mV$	[231]
$Fe_{60}Co_{20}Si_{10}B_{10}$	30% KOH, 70 °C	$77\,mV\,dec^{-1}$	$\eta_{250} = 157\,mV\,dec^{-1}$	[232]
$Fe_{58}Co_{26}Si_7B_9$ nanocryst.	30% KOH, 70 °C	$73\,mV\,dec^{-1}$	$\eta_{250} = 181\,mV\,dec^{-1}$	[232]
$Fe_{40}Ni_{40}B_{20}$	1 M KOH, 90 °C	$188\,mV\,dec^{-1}$	$\eta_{300} = 488\,mV$	[231]
$Cu_{70}Ti_{30}$	1 M KOH, 90 °C	$248\,mV\,dec^{-1}$	$\eta_{300} = 600\,mV$	[231]
$Ni_{80}Mo_{20}$ nanocryst.	1 M NaOH, 60 °C	$320\,mV\,dec^{-1}$	$\eta_{100} = 150\,mV$	[59]
Ti_2RuFe nanocryst.	1 M NaOH, 24 °C	$160\,mV\,dec^{-1}$	$\eta_{100} = 100\,mV$	[234]

are characterized by high electrocatalytic activity with $\eta_{400} = 100\,mV$ at 80 °C in H_2SO_4, HCl and HBr.[221] This value is similar to that obtained using Pt activated graphite electrodes.

6 HYDROGEN EVOLUTION ON AMORPHOUS AND NANO-CRYSTALLINE MATERIALS

Amorphous metals, also known as metallic glass alloys, represent a new class of metallic materials.[7] They differ from the traditional metals in that they have a noncrystalline structure and possess unique physical and magnetic properties that combine strength and hardness with flexibility and toughness. They also have different chemical proprieties such as corrosion resistance and electrocatalytic activities.[222] Amorphous metastable alloys may be fabricated in almost any composition. As the electronic properties of solids depend on their structure it is expected that new catalytically active materials could be prepared in such an amorphous form. Amorphous alloys often contain ~20% of metalloid(s) (B, Si, P, Ge). They are prepared by fast solidification (melt-quenching, spin-coating), sputtering, or electrodeposition. Phosphorus, sulfur and boron containing amorphous alloys were described in Sections 5.5–5.7.

Fe/Zr, Ni/Zr, Co/Zr amorphous alloys showed hydrogen overpotential similar to pure metals or simple mixtures, Ni/Nb and Co/Nb alloys showed higher hydrogen overpotential and only Cu/Ti alloys ($Cu_{70}Ti_{30}$) lower overpotential.[223] Other studies of $Cu_{50}Ti_5$, $Cu_{35}Ti_{65}$ and $Cu_{33}Zr_{67}$ have shown that surface activation in 1 M HF increases activity of these alloys.[224] In this case leaching of Ti or Zr and their oxides produces porous surface and the observed increased activity is caused by the increase in the real surface area.

Ni/Zr alloys were prepared by melt-quenching[225, 226] and mechanical alloying and pressing of produced powders.[227] Their activities are displayed in Table 10. Activity of amorphous pressed powders was larger but fast deactivation accompanied by formation of black film and large crevices was observed. These effects are due to hydrogen absorption. Similar deactivation was observed for the amorphous alloys of $(Ni_xCo_{1-x})_yZr_{1-y}$,[228] $Ni_{65}Nb_{35}$, and $Ni_{65}Al_{10}B_{25}$[229]. Tafel slopes of freshly prepared alloys are often large due to presence of an oxide film at the electrode surface.[230]

Several amorphous materials (Fe, Ni, Co, Mo, Pd, Cu)+(Ti, Si, B, P) have been studied by Kreysa and Håkansson.[231] They showed that $Fe_{60}Co_{20}Si_{10}B_{10}$ exhibit even higher activity than polycrystalline Pt (although in alkaline solutions Pt is highly deactivated) (Table 10). Its activity stays high in the industrial electrolysis conditions.[232] On the other hand, alloys $Ni_{72}Co_x metalloid_{20}$ did not show any special electrocatalytic activities.[233]

Nanocrystalline Ti_2RuFe prepared by ball milling technique is quite active for the HER.[234] Irreversible transformation of the surface morphology occurred during hydride formation and increased significantly the active surface area.

It is evident from Table 10 that amorphous or nanocrystalline alloys do not show any extraordinary electrocatalytic properties. Moreover, they are usually covered by an oxide layer and must be activated with HF, which increases their real surface area. They are often deactivated during HER and tend to crystallize during heat treatment. Applications of glassy alloys for the HER are also limited because of their cost, limitations of shape and size, and stability.

Ultra-fine metal particles seem to be an interesting candidate for the HER. Ezaki *et al*.[235] used ultra-fine particles of Ni (100 nm diameter) and Mo (30 nm) prepared by d.c. thermal plasma spraying. In acid solutions sintered Ni and Ni/Mo particles show activities close to that of polycrystalline platinum. The addition of 10% of Mo increases electrode activity towards the HER.

7 SOLID POLYMERS WATER ELECTROLYSIS

The concept of solid polymer water electrolysis was developed by General Electric in 1970s.[4, 236, 237] It is a simple idea of carrying pure water electrolysis by using proton conducting membrane covered with electrocatalytic layers on both sides. This is, in fact, an inverse process to that used in the polymer electrolyte fuel cells. Solid polymer acts as an electrolyte. The electrocatalysts are dispersed and impregnated into the membrane and hydrogen/oxygen evolution takes place on both sides of the membrane. As an electrolyte perfluorosulfonated cationic exchange Nafion or other proton exchange membranes are usually used,[238] although OH^- conducting membranes have also been studied.[239] Finely dispersed Pt[240–242] or IrO_2/Ti[240] materials are used as cathodes because the membrane is strongly acidic. A pressurized electrolyzer working at 15 bar has also been developed.[243] These electrolyzers work at high current densities of 2 A cm^{-2} [242] to 10 A cm^{-2}.[244]

8 HIGH TEMPERATURE OR PRESSURE ELECTROLYSIS

Ordinary water electrolysis is conducted at 70–90 °C under atmospheric pressure.[4] It is advantageous to electrolyze water at higher temperatures and pressures since this increases the kinetics of electrode reactions (reduction of overpotential), decreases the size of hydrogen bubbles, and decreases the ohmic drop in the solution. Increase of pressure is also advantageous since this avoids the additional work of compressing the gases produced for storage. However, electrical energy must be supplied to the electrolyzer to heat water and water vapor leaving the electrolyzer together with H_2 and O_2 and compress the gases formed. Water electrolysis is often carried out at temperatures of 100–150 °C and pressures up to 30 atm.[4, 245–249] Electrolysis at intermediate temperatures (600–700 K) in molten hydroxides has also been tested.[250]

Steam electrolysis at high temperatures (700–1100 °C) is an inverse process to power generation in the solid oxide fuel cells (SOFC).[4, 251] Water electrolysis was carried out at 900 °C in cells containing yttria stabilized zirconia (YSZ)[4, 252–254] or a ceria-doped YSZ[257] thin layer solid electrolyte. Pt,[253] Pt/CeO_{2-x},[256] Ni cermet,[254] and strontium doped lanthanum chromate, $La_{0.8}Sr_{0.2}CrO_3$,[257] were used as cathodes. However, steam electrolysis demands costly water heating to high temperatures. SOFC based commercial electrolyzers have been built by Lurgi and Westinghouse.[258]

9 ELECTRODE MATERIALS FOR HER IN ACID MEDIA

Water electrolysis is usually carried out in alkaline solutions because of the difficulties of finding inexpensive anodes stable in acidic solutions. The cathode materials must also be immune to current interruptions. The most active materials for the HER in acid media are of course noble metals. Between other electrocatalytic materials are Ru and Ir oxides, tungsten carbide and heteropolyacid modified electrodes. Their activity was described in the chapters above.

10 CONCLUSION

Electrocatalysis of the hydrogen evolution reaction has been studied on many metals, alloys and composites. Many very active materials have been developed and applied in industrial water electrolysis in advanced electrolyzers. Between the most active materials are noble metals, doped Raney-type alloys, IrO_2/Ru_2O, sulfides, borides, and Ni/Mo based alloys. Unfortunately, noble metals are very expensive and easily poisoned and their activity decreases with time. Recently, studies on well-defined surfaces have been carried out in clean conditions. However, these results do not explain behavior of polycrystalline and rough/porous surfaces. Although there are many papers reporting Tafel parameters, there have not been many reliable studies of the detailed mechanism and kinetics of this processes. Very often contradictory data are published. Many of these problems are related to the difficulty of preparation of clean electrodes and solutions, especially in alkaline media.

Besides, many researchers are interested in the activity of the final product and do not carry out any mechanistic studies. Often it is difficult to know whether the surface roughness or intrinsic activity contributes more to the apparent electrode activity. Studies of several nickel-based materials have revealed that the main contribution to the electrocatalytic activity comes from the increase of the real surface roughness.[259] On the other hand, alloying Ni with Mo produces evident electrocatalytic effect. Many materials may still be improved and optimized. Details of the mechanism and kinetics of the HER on these materials have still to be investigated. For better insight, individual contributions of the surface roughness and the intrinsic electrocatalytic properties to the overall kinetics of the HER on these materials should be determined.

REFERENCES

1. J. P. Hoare, 'Standard Potentials in Aqueous Solutions', A. J. Bard, R. Parsons and J. Jordan (Eds), Marcel Dekker, New York, p. 51 (1984).
2. R. L. LeRoy, C. T. Bowen and D. J. LeRoy, *J. Electrochem. Soc.*, **127**, 1954 (1980).
3. R. L. LeRoy, *Int. J. Hydrogen Energy*, **8**, 401 (1983).
4. B. V. Tilak, P. W. T. Lu, J. E. Colman and S. Srinivasan, 'Comprehensive Treatise of Electrochemistry', J. O'M. Bockris, B. E. Conway, E. Yeager and R. E. White (Eds), Plenum, New York, Vol. 2, p. 1 (1981).
5. A. J. Appleby, H. Kita, M. Chemla and G. Bronoel, 'Encyclopedia of Electrochemistry of the Elements', Vol. 9A, p. 383 (1982).
6. H. Wendt (Ed), 'Electrochemical Hydrogen Technologies', Elsevier, Amsterdam, 1990.
7. S. Trasatti, 'Advances in Electrochemical Science and Engineering', H. Gerischer and C. W. Tobias (Eds), VCH, Weinheim, Vol. 2, p. 2 (1992).
8. B. V. Tilak, A. C. Ramamurthy and B. E. Conway, *Proc. Indian Acad. Sci. (Chem. Sci.)*, **97**, 359 (1986).
9. A. Lasia, *J. Electroanal. Chem.*, **454**, 115 (1998).
10. K. A. Gschneidner, 'Solid State Physics', F. Seitz and D. Turnbull (Eds), Vol. 16, Academic Press, New York, p. 275 (1964).
11. M. M. Jaksic, *Int. J. Hydrogen Energy*, **26**, 559 (2001).
12. R. Parsons, *Trans. Farad. Soc.*, **54**, 1053 (1958).
13. A. Lasia, *Can. J. Chem.*, **75**, 1615 (1997).
14. S. Trasatti, *J. Electroanal. Chem.*, **39**, 163 (1972).
15. B. E. Conway and G. Jerkiewicz, *Electrochim. Acta*, **45**, 4075 (2000).
16. O. A. Petrii and G. A. Tsirlina, *Electrochim. Acta*, **39**, 1739 (1994).
17. A. J. Appleby, 'Comprehensive Treatise of Electrochemistry', B. E. Conway, J. O'M. Bockris, E. Yeager, S. U. M. Khan and R. E. White (Eds), Plenum Press, New York, Vol. 7, p. 173 (1983).
18. P. Dabo, H. Ménard and P. Trembly, *J. Appl. Electrochem.*, **28**, 601 (1998).
19. Southampton Electrochemistry Group, 'Instrumental Methods in Electrochemistry', Ellis Horwood, p. 239 (1985).
20. J. Barber, S. Morin and B. E. Conway, *J. Electroanal. Chem.*, **446**, 125 (1998).
21. B. E. Conway, J. Barber and S. Morin, *Electrochim. Acta*, **44**, 1109 (1998).
22. N. M. Marković, B. N. Grugur and P. N. Ross, *J. Phys. Chem.*, **101**, 5405 (1997).
23. G. Kokkinidis, A. Papoutsis, D. Stoychev and A. Milchev, *J. Electroanal. Chem.*, **486**, 48 (2000).
24. (a) A. Matsuda and R. Notoya, *J. Res. Inst. Catal. Hokkaido Univ.*, **14**, 165 (1966); (b) A. Matsuda, T. Ohmori, K. Kunimatsu and T. Kushimoto, *J. Res. Inst. Catal. Hokkaido Univ.*, **24**, 187 (1976).
25. T. Yamazaki and M. Enyo, *Electrochim. Acta*, **35**, 523 (1990).
26. J. Y. Huot and L. Brossard, *Int. J. Hydrogen Energy*, **12**, 821 (1987).
27. L. Brossard, *Int. J. Hydrogen Energy*, **16**, 13 (1991).
28. P.-P. Grand, 'PhD Thesis', Université de Sherbrooke, Québec, Canada (2001).
29. M. M. Jaksic, J. Brun, B. Johansen and R. Tunold, *Russ. J. Electrochem.*, **31**, 1187 (1995).
30. C. Hitz and A. Lasia, *J. Electroanal. Chem.*, **500**, 213 (2001).
31. G. Tabbone and A. Lasia, unpublished results (2001).
32. D. M. Soares, O. Teschke and I. Torriani, *J. Electrochem. Soc.*, **139**, 98 (1992).
33. M. Bernardini, N. Comisso, G. Mengoli and L. Sinico, *J. Electroanal. Chem.*, **457**, 205 (1998).
34. R. Juškènas, A. Selskis and V. Kadziauskinè, *Electrochim. Acta*, **43**, 1903 (1998).
35. A. Lasia and A. Rami, *J. Electroanal. Chem.*, **294**, 123 (1990).
36. C. Hitz, 'PhD Thesis', Université de Sherbrooke, Québec, Canada (2001).
37. J. Moran, Jr, 'PhD Thesis', University of Virginia (1980).
38. I. Abe, T. Fujimaki and M. Matsubara, 'Hydrogen Energy Progress IV', in "Proceedings World Hydrogen Energy Conference", Pasadena, Vol. 1, p. 239 (1982).
39. I. Abe, T. Fujimaki and M. Matsubara, *Int. J. Hydrogen Energy*, **9**, 753 (1984).
40. P. Los and A. Lasia, *J. Electroanal. Chem.*, **333**, 115 (1992).
41. J. Y. Huot and L. Brossard, *J. Appl. Electrochem.*, **18**, 815 (1988).
42. R. M. Aboutallah, D. W. Kirk, S. J. Thorpe and J. W. Graydon, *J. Electrochem. Soc.*, **148**, E357 (2001).
43. G. Kreysa, B. Hakansson and P. Ekundge, *Electrochim. Acta*, **33**, 1351 (1988).

44. M. F. Kibria, M. Sh. Mridha and A. H. Khan, *Int. J. Hydrogen Energy*, **20**, 435 (1995).
45. G. Tabbone, C. Hitz and A. Lasia, unpublished data (2001).
46. J. Arold and J. Tamm, *Soviet Electrochem.*, **25**, 369 (1987).
47. M. H. Miles, G. Kissel, P. W. T. Lu and S. Srinivasan, *J. Electrochem. Soc.*, **123**, 332 (1976).
48. L. B. Albertini, A. C. D. Angelo and E. R. Gonzalez, *J. Appl. Electrochem.*, **22**, 888 (1992).
49. L. Brewer, 'Electronic Structure and Alloy Chemistry of Transition Elements', P. A. Beck (Ed), Interscience, New York, p. 221 (1963).
50. M. M. Jakšić, *J. Molec. Catal.*, **38**, 161 (1986).
51. M. M. Jaksic, C. M. Lacnjevac, B. N. Grgur and N. V. Krstajic, *J. New Mater. Electrochem. Syst.*, **3**, 131 (2000).
52. A. Bélanger and A. K. Vijh, *Int. J. Hydrogen Energy*, **12**, 227 (1987).
53. E. R. Gonzalez, G. Tremiliosi-Filho and M. J. Giz, *Curr. Top. Electrochem.*, **2**, 167 (1993).
54. D. E. Brown, M. N. Mahmood, M. C. M. Man and A. K. Turner, *Electrochim. Acta*, **29**, 1551 (1984).
55. D. E. Brown and M. N. Mahmood, US Patent 4,358,475 (1982).
56. I. Arul Raj and V. K. Venkatesan, *Int. J. Hydrogen Energy*, **13**, 215 (1988).
57. J. Divisek, H. Schmitz and J. Balej, *J. Appl. Electrochem.*, **19**, 519 (1989).
58. J. Y. Huot, M. L. Trudeau and R. Schultz, *J. Electrochem. Soc.*, **138**, 1316 (1991).
59. P. Kedzierzawski, D. Oleszak and M. Janik-Czachor, *Mater. Sci. Eng.*, **A300**, 105 (2001).
60. J. M. Jakšić, M. V. Vojnović and N. V. Krstajić, *Electrochim. Acta*, **45**, 4151 (2000).
61. J. Z. O. Stachurski, D. Pouli, J. A. Ripa and G. F. Pokrzyk, US Patent 4,354,915 (1982).
62. B. E. Conway and L. Bai, *Int. J. Hydrogen Energy*, **11**, 533 (1986).
63. R. Šimpraga, L. Bai and B. E. Conway, *J. Appl. Electrochem.*, **25**, 628 (1995).
64. I. Arul Raj, *Int. J. Hydrogen Energy*, **17**, 413 (1992).
65. M. B. F. Santos, E. Peres da Silva, R. Andrade, Jr and J. A. F. Dias, *Electrochim. Acta*, **37**, 29 (1992).
66. H. Yamashita, T. Yamamura and K. Yoshimoto, *J. Electrochem. Soc.*, **140**, 2238 (1993).
67. A. Stephen, D. Kalpana, M. V. Ananth and V. Ravichandran, *Int. J. Hydrogen Energy*, **24**, 1059 (1999).
68. C. Fan and D. L. Piron, *Surf. Coat. Technol.*, **73**, 91 (1995).
69. N. V. Krstajić, B. N. Grgur, N. S. Mladenović, M. V. Vojnović and M. M. Jakšić, *Electrochim. Acta*, **42**, 323 (1997).
70. D. E. Hall, J. M. Sarver and D. O. Gothard, *Int. J. Hydrogen Energy*, **13**, 547 (1988).
71. A. C. D. Angelo and A. Lasia, in "Proceedings of the 7th Canadian Hydrogen Workshop", S. K. Mehta and T. K. Bose (Eds), Canadian Hydrogen Association, p. 365 (1995).
72. R. Bocutti, M. J. Saeki, A. O. Florentino, C. L. F. Oliveira and A. C. D. Angelo, *Int. J. Hydrogen Energy*, **25**, 1051 (2000).
73. W. Hu and J.-Y. Lee, *Int. J. Hydrogen Energy*, **23**, 253 (1998).
74. W. H. Hu, X. Cao, F. Wang and Y. Zhang, *Int. J. Hydrogen Energy*, **22**, 621 (1997).
75. W. Hu, *Int. J. Hydrogen Energy*, **25**, 111 (2000).
76. H. Kronenberger, Ch. Fabjan and G. Frithum, *Int. J. Hydrogen Energy*, **16**, 219 (1991).
77. H. Dumond, P. W. Wrona, J. M. Lalancette and H. Ménard, *J. Appl. Electrochem.*, **22**, 1049 (1992).
78. P. Los, A. Lasia, H. Ménard and L. Brossard, *J. Electroalan. Chem.*, **360**, 101 (1993).
79. H. Dumond, P. Los, A. Lasia and H. Ménard, *J. Appl. Electrochem.*, **23**, 684 (1993).
80. H. Dumond, P. Los, L. Brossard, A. Lasia and H. Ménard, *J. Electrochem. Soc.*, **139**, 2143 (1992).
81. Y. Kungi, T. Nonaka, Y.-B. Chong and N. Watanabe, *Electrochim. Acta*, **37**, 353 (1992).
82. (a) A. C. C. Tseung and P. R. Vassie, *Electrochim. Acta*, **20**, 759 (1975); (b) A. C. C. Tseung and P. R. Vassie, *Electrochim. Acta*, **20**, 763 (1975); (c) A. C. C. Tseung and P. R. Vassie, *Electrochim. Acta*, **21**, 315 (1976).
83. J. J. Borodziński and A. Lasia, *Int. J. Hydrogen Energy*, **18**, 985 (1993).
84. H. J. Miao and D. L. Piron, *Electrochim. Acta*, **38**, 1079 (1993).
85. P. Dabo, H. Ménard and L. Brossard, *Int. J. Hydrogen Energy*, **22**, 763 (1997).
86. J. Fournier, P. K. Wrona, A. Lasia, R. Lacasse, J.-M. Lalancette and H. Ménard, *J. Electrochem. Soc.*, **139**, 2372 (1992).
87. P. Dabo, J. Fournier, L. Brossard, H. Ménard, P. Magny and B. Mahdavi, *Int. J. Hydrogen Energy*, **23**, 167 (1998).
88. L. Chen and A. Lasia, *J. Electrochem. Soc.*, **139**, 3458 (1992).
89. A. Kawashima, T. Sakaki, H. Habazaki and K. Hashimoto, *Mater. Sci. Eng.*, **A267**, 246 (1999).
90. O. Savadogo and S. Thibault, *Int. J. Hydrogen Energy*, **14**, 865 (1989).
91. O. Savadogo and D. L. Piron, *Int. J. Hydrogen Energy*, **15**, 715 (1990).
92. O. Savadogo and E. Forget, *Int. J. Hydrogen Energy*, **16**, 665 (1991).
93. O. Savadogo, S. Lévesque, E. Ndzbet, A. Martel and J. Lessard, *Int. J. Hydrogen Energy*, **17**, 101 (1994).
94. O. Savadogo, F. Carrier and E. Forget, *Int. J. Hydrogen Energy*, **19**, 429 (1994).
95. O. Savadogo and H. Lavoie, *Int. J. Hydrogen Energy*, **17**, 473 (1992).
96. O. Savadogo and G. Bartolacci, *Int. J. Hydrogen Energy*, **17**, 109 (1992).
97. O. Savadogo, K. Amzugar and D. L. Piron, *Int. J. Hydrogen Energy*, **15**, 783 (1990).

98. E. Ndzebet and O. Savadogo, *Int. J. Hydrogen Energy*, **20**, 636 (1995).
99. O. Savadogo and E. Ndzebet, *Int. J. Hydrogen Energy*, **26**, 213 (2001).
100. M. Raney, US Patent 1,628,191 (1927).
101. E. Justi, A. Winsel, G. Grünbergm, H. Spengler and W. Vielstich, German Patent, 1,065,821 (1957).
102. W. Vielstich, *Chem. Ing. Technol.*, **33**, 75 (1961).
103. P. Fouilloux, *Appl. Catal.*, **8**, 1 (1983).
104. J. Lessard and G. Belot, US Patent 4,584,069 (1986).
105. Y. Choquette, H. Ménard and L. Brossard, *Int. J. Hydrogen Energy*, **15**, 1 (1990).
106. J. Freel, W. J. M. Pieters and R. B. Anderson, *J. Catal.*, **14**, 247 (1969).
107. J.-M. Ménard, Y. Trambouze and M. Prettre, *Bull. Soc. Chim. France*, 401 (1963).
108. M. L. Bakker, D. J. Young and M. S. Wainwright, *J. Mater. Sci.*, **23**, 3921 (1988).
109. V. R. Choudhary, S. K. Chaudhari and A. N. Gokarn, *Ind. Eng. Chem. Res.*, **28**, 33 (1989).
110. Y. Choquette, L. Brossard and H. Ménard, *J. Appl. Electrochem.*, **29**, 855 (1990).
111. S. Tanaka, N. Hirose and T. Tanaki, *Denki Kagaku*, **12**, 1044 (1997).
112. O. S. Abramzon, S. F. Chernyshov and A. G. Pshenichnikov, *Soviet Electrochem.*, **12**, 1520 (1976).
113. E. Endoh, H. Otouma, T. Morimoto and Y. Oda, *Int. J. Hydrogen Energy*, **12**, 473 (1987).
114. Y. Choquette, H. Ménard and L. Brossard, *Int. J. Hydrogen Energy*, **14**, 637 (1989).
115. N. Yoshida, M. Yoshitake, E. Endoh and T. Morimito, *Int. J. Hydrogen Energy*, **14**, 137 (1989).
116. D. E. Hall, *J. Appl. Electrochem.*, **14**, 107 (1984).
117. K. Lohrberg and P. Kohl, *Electrochim. Acta*, **29**, 1557 (1984).
118. G. Schiller and V. Borck, *Int. J. Hydrogen Energy*, **17**, 261 (1992).
119. D. Miousse, A. Lasia and V. Borck, *J. Appl. Electrochem.*, **25**, 592 (1995).
120. J. Fournier, D. Miousse and J.-G. Legoux, *Int. J. Hydrogen Energy*, **24**, 519 (1999).
121. H. Wendt, H. Hoffmann and V. Plazak, *Mater. Chem. Phys.*, **22**, 27 (1989).
122. K. Lohrberg, H. Wüllenweber, J. Müller and B. Sermond, US Patent 4,278,568.
123. C. R. S. Needes, US Patent 4,116,804.
124. L. Chen and A. Lasia, *J. Electrochem. Soc.*, **140**, 2464 (1993).
125. E. Justi, A. Winsel, H. Spengler and W. Vielstich, German Patent 1065821 (1957).
126. A. Rami and A. Lasia, *J. Appl. Electrochem.*, **22**, 376 (1992).
127. P. Los, A. Rami and A. Lasia, *J. Appl. Electrochem.*, **23**, 135 (1993).
128. G. Schiller, R. Henne and V. Borck, *J. Thermal Spray Technol.*, **4**, 185 (1995).
129. S. Tanaka, N. Hirose, T. Tanaki and H. Ogata, *J. Electrochem. Soc.*, **147**, 2242 (2000).
130. Y. Choquette, L. Brossard and H. Ménard, *Int. J. Hydrogen Energy*, **15**, 551 (1990).
131. K. Schultze and H. Bartlet, *Int. J. Hydrogen Energy*, **17**, 711 (1992).
132. H. Ewe, E. Justi and A. Schmitt, *Electrochim. Acta*, **19**, 799 (1974).
133. K. Mund, G. Richter and F. von Sturm, *J. Electrochem. Soc.*, **124**, 1 (1977).
134. T. Kenjo, *J. Electrochem. Soc.*, **132**, 383 (1985).
135. T. Kenjo, *Electrochim. Acta*, **33**, 41 (1988).
136. S. Tanaka, N. Hirose and T. Tanaki, *J. Electrochem. Soc.*, **146**, 2477 (1999).
137. S. Tanaka, N. Hirose and T. Tanaki, *Int. J. Hydrogen Energy*, **25**, 481 (2000).
138. J. K. Depo, M. Okido, G. A. Capuano and R. Harris, *Can. Metallurgical. Quart.*, **33**, 369 (1994).
139. A. Kayser, V. Borck, M. von Bradke, R. Henne, W. Kaysser and G. Schiller, *Z. Metallkd.*, **83**, 656 (1992).
140. L. Birry and A. Lasia, 'Studies of the hydrogen evolution reaction on Raney nickel–molybdenum electrodes', Presented at 4th International Symposium on New Materials for Electrochemical Systems, Montréal, July (2001).
141. N. Yoshida, M. Yoshitake, E. Endoh and T. Moromoto, *Int. J. Hydrogen Energy*, **14**, 137 (1989).
142. N. V. Korovin, N. I. Kozlova and O. N. Savel'eva, *Sov. Electrochem.*, **14**, 1366 (1978).
143. S. Rausch and H. Wendt, *J. Electrochem. Soc.*, **143**, 2852 (1996).
144. (a) S. Swathirayan, *J. Electrochem. Soc.*, **133**, 671 (1986); (b) S. Swathirayan, *J. Electroanal. Chem.*, **221**, 211 (1987).
145. F. Elkhatabi, M. Benballa, M. Sarret and C. Müller, *Electrochim. Acta*, **44**, 1645 (1999).
146. J. Baley, J. Divisek, H. Schmitz and J. Mergel, *J. Appl. Electrochem.*, **22**, 705, 711 (1992).
147. B. N. Popov, M. Ramasubramanian, S. N. Popova, R. E. White and K.-M. Yin, *J. Chem. Soc., Faraday Trans.*, **92**, 4021 (1996).
148. D. E. Hall, *Plat. Surf. Finish.*, **70**, 59 (1983).
149. T. Boruciński, S. Rausch and H. Wendt, *J. Appl. Electrochem.*, **22**, 1031 (1992).
150. L. Chen and A. Lasia, *J. Electrochem. Soc.*, **138**, 3321 (1991).
151. M. J. de Giz, S. A. S. Machado, L. A. Avaca and E. R. Gonzalez, *J. Appl. Electrochem.*, **22**, 973 (1992).
152. M. B. F. Santos, E. Peres da Silva, R. Andrade, Jr and J. A. F. Dias, *Electrochim. Acta*, **37**, 29 (1992).
153. S. A. S. Machado, J. Tiengo, P. de Lime Neto and L. A. Avaca, *J. Appl. Electrochem.*, **26**, 431 (1996).

154. H. B. Suffredini, J. L. Cerne, F. C. Crnkovic, S. A. S. Machado and L. A. Avaca, *Int. J. Hydrogen Energy*, **25**, 415 (2000).
155. M. J. Giz, S. C. Bento and E. R. Gonzalez, *Int. J. Hydrogen Energy*, **25**, 621 (2000).
156. R. Karimi Shervedani and A. Lasia, *J. Electrochem. Soc.*, **144**, 2652 (1997).
157. R. Karimi Shervedani and A. Lasia, *J. Appl. Electrochem.*, **29**, 979 (1999).
158. L. Brossard, *Int. J. Hydrogen Energy*, **13**, 315 (1988).
159. R. de Levie, 'Advances in Electrochemistry and Electrochemical Engineering', P. Delahay (Ed), Interscience, New York, Vol. 6, p. 329 (1967).
160. A. Lasia, *J. Electroanal. Chem.*, **397**, 27 (1995).
161. A. Lasia, *J. Electroanal. Chem.*, **454**, 115 (1998).
162. S. Trasatti, 'Electrochemistry of Novel Materials', J. Lipkowski and P. N. Ross (Eds), VCH, New York, p. 207 (1994).
163. J.-P. Diard, B. LeGorrec and S. Maximovich, *Electrochim. Acta*, **35**, 1099 (1990).
164. S. Trasatti, 'Modern Chlor-Alkali Technology', T. C. Wellington (Ed), Elsevier, Amsterdam, p. 281 (1992).
165. 'Electrodes of Conductive Metallic Oxides', Parts A and B, S. Trasatti (Ed), Elsevier, Amsterdam (1980, 1981).
166. E. R. Kötz and S. Stucki, *J. Appl. Electrochem.*, **17**, 1190 (1987).
167. M. Klejin and H. P. van Leeuwen, *J. Electroanal. Chem.*, **247**, 253 (1988).
168. C. Iwakura, M. Tanaka, S. Nakamutsu and H. Inoue, *Electrochim. Acta*, **40**, 977 (1995).
169. D. Miousse and A. Lasia, *J. New Mater. Electrochem. Syst.*, **2**, 71 (1999).
170. A. C. Tavares and S. Trasatti, *Electrochim. Acta*, **45**, 4195 (2000).
171. I. M. Kodintsev, S. Trasatti, M. Rubel, A. Wieckowski and N. Kaufher, *Langmuir*, **8**, 283 (1992).
172. M. Blouin and D. Guay, 'Electrode Materials and Processes for Energy Storage and Conversion', in "The Electrochemical Society Proceedings" S. Srinivasan, D. D. Macdonald and A. C. Khandkar (Eds), Pennington, NJ, PV94-23, p. 396, (1994); M. Blouin and D. Guay, *J. Electrochem. Soc.*, **144**, 573 (1997).
173. L. Chen, D. Guay, F. H. Pollak and F. Lévy, *J. Electroanal. Chem.*, **429**, 185 (1997).
174. T. Hepel, F. H. Pollak and W. E. O'Grady, *J. Electrochem. Soc.*, **131**, 2094 (1984).
175. S. Ardizzone, G. Fregonara and S. Trasatti, *Electrochim. Acta*, **35**, 263 (1990).
176. Y. Mo, W.-B. Cai, J. Dong, P. R. Carey and D. A. Scherson, *Electrochem. Solid State Lett.*, **4**, E37 (2001).
177. Pauporté, F. Andolfatto and R. Durand, *Electrochim. Acta*, **45**, 431 (1999).
178. I. M. Kodintsev and S. Trasatti, *Electrochim. Acta*, **39**, 1803 (1994).
179. L. Chen, D. Guay and A. Lasia, *J. Electrochem. Soc.*, **143**, 3576 (1996).
180. H. Chen and S. Trasatti, *J. Electroanal. Chem.*, **357**, 91 (1993).
181. E. Veggetti, I. M. Kodintsev and S. Trasatti, *J. Electroanal. Chem.*, **339**, 255 (1992).
182. A. Anani, Z. Mao, S. Srinivasan and A. J. Appleby, *J. Appl. Electrochem.*, **21**, 683 (1991).
183. H. Vanbenborre, P. Vermeiren and R. Leysen, *Electrochim. Acta*, **29**, 297 (1984).
184. I. Paseka, *Electrochim. Acta*, **38**, 2449 (1993).
185. E. R. Gonzalez, L. A. Avaca, G. Temiliosi-Filho, S. A. S. Machado and M. Ferreira, *Int. J. Hydrogen Energy*, **19**, 17 (1994).
186. A. Nidola and R. Schira, *Int. J. Hydrogen Energy*, **11**, 449 (1986).
187. T. Borucinsky, S. Rausch and H. Wendt, *J. Appl. Electrochem.*, **27**, 762 (1997).
188. N. A. Assunção, M. J. de Giz, G. Tremiliosi-Filho and E. R. Gonzalez, *J. Electrochem. Soc.*, **144**, 2794 (1997).
189. E. B. Castro, M. J. de Giz, E. R. Gonzalez and J. R. Vilche, *Electrochim. Acta*, **42**, 951 (1997).
190. T. Våland, T. Burchardt and S. F. van der Meer, *Corrosion Sci.*, **43**, 147 (2001).
191. A. C. C. Tseung, J. A. Antonian and D. B. Hibert, *Chem. Ind.*, 54 (1984).
192. H. Vandenborre, R. Leysen and H. Nackaerts, *Int. J. Hydrogen Energy*, **8**, 81 (1983).
193. N. A. Vante, B. Schubert, H. Tributsch and A. Perrin, *J. Catal.*, **112**, 384 (1988).
194. E. Tóth-Kádár, I. Bakonyi, A. Sólyom, J. Hering, G. Konczos and F. Pavlyák, *Surf. Coat. Technol.*, **31**, 31 (1987).
195. R. Karimi Shervedani and A. Lasia, *J. Electrochem. Soc.*, **144**, 511 (1997).
196. T. Morikawa, T. Nakade, M. Yokoi, Y. Fukumoto and C. Iwakura, *Electrochim. Acta*, **42**, 115 (1997).
197. C.-C. Hu and A. Bai, *J. Appl. Electrochem.*, **31**, 565 (2001).
198. J. J. Podesta, R. C. V. Piatti, A. J. Arvia, P. Ekundge, K. Jüttner and G. Kreysa, *Int. J. Hydrogen Energy*, **17**, 9 (1992).
199. S. Yoshida, H. Yamashita, T. Funabiki and T. Yonezawa, *J. Chem. Soc. Chem. Commun.*, 964 (1982).
200. R. L. Zeller, III and U. Landau, *J. Electrochem. Soc.*, **139**, 3464 (1992).
201. M. E. Touhami, M. Cherakaoui, A. Srhiri, A. B. Bachir and E. Chassaing, *J. Appl. Electrochem.*, **26**, 478 (1996).
202. N. V. Sotskaya, L. G. Goncharova, T. A. Kravchenko and E. V. Zhivotova, *Russ. J. Electrochem.*, **33**, 529 (1997).
203. M. E. Touhami, E. Chassaing and M. Cherakaoui, *Electrochim. Acta*, **43**, 1721 (1998).
204. A. Królikowski and P. Butkiewicz, *Electrochim. Acta*, **38**, 1979 (1993).
205. P. K. Ng, D. D. Snyder and J. Lasala, *J. Electrochem. Soc.*, **135**, 1376 (1988).

206. T. Burchardt, V. Hansen and T. Våland, *Electrochim. Acta*, **46**, 2761 (2001).
207. I. Bakonuyi, A. Cziráki, I. Nagy and M. Hossó, *Zeit. Metallkunde*, **77**, 425 (1986).
208. I. Paseka, *Electrochim. Acta*, **40**, 1633 (1995).
209. I. Paseka and J. Velicka, *Electrochim. Acta*, **42**, 237 (1997).
210. I. Paseka, *Electrochim. Acta*, **44**, 4551 (1999).
211. T. Burchardt, *Int. J. Hydrogen Energy*, **25**, 627 (2000).
212. R. Karimi Shervedani, 'Thesis', Université de Sherbrooke (1997).
213. D. E. Mears and M. Boudart, *A. I. Ch. E. J.*, **12**, 313 (1966).
214. J. Saida, A. Inoue and T. Masumoto, *Metallurg. Trans. A*, **22A**, 2125 (1991).
215. B. Mahdavi, P. Los, M. J. Lessard and J. Lessard, *Can. J. Chem.*, **72**, 2268 (1994).
216. B. Mahdavi, P. Chambrion, J. Binette, E. Martel and J. Lessard, *Can. J. Chem.*, **73**, 846 (1995).
217. J. J. Borodzinski and A. Lasia, *J. Appl. Electrochem.*, **24**, 1267 (1994).
218. A. K. Vijh, G. Bélanger and R. Jacques, *Int. J. Hydrogen Energy*, **17**, 479 (1992).
219. A. K. Vijh, G. Bélanger and R. Jacques, *Int. J. Hydrogen Energy*, **15**, 789 (1990).
220. I. Nikolov, K. Petrow, T. Vitanov and A. Guschev, *Int. J. Hydrogen Energy*, **8**, 437 (1983).
221. B. D. Struck, H. Neumeister and A. Naumidis, *Int. J. Hydrogen Energy*, **11**, 541 (1986).
222. M. D. Archer, C. C. Corke and B. H. Harji, *Electrochim. Acta*, **32**, 13 (1987).
223. M. Naka, K. Hasimoto, T. Masumoto and I. Okamoto, in 'Proceedings 4th International Conference on Rapidly Quenched Metals', T. Matsumoto and K. Suzuki (Eds), Japan Institute of Metals, Sendai, p. 1431 (1982).
224. K. Machida, M. Enyo, K. Kai and K. Suzuki, *J. Less-Common Met.*, **100**, 377 (1984).
225. J.-Y. Huot and L. Brossard, *Int. J. Hydrogen Energy*, **12**, 599 (1987).
226. M. Metikoš-Huković and A. Jukić, *Electrochim. Acta*, **45**, 4159 (2000).
227. J. Y. Huot, M. Trudeau and R. Schultz, *Int. J. Hydrogen Energy*, **15**, 287 (1990).
228. J. Y. Huot, A. van Neste, L. Brossard and R. Schultz, *Surf. Coat. Technol.*, **35** 241 (1988).
229. J.-Y. Huot, M. Trudeau, L. Brossard and R. Schultz, *Int. J. Hydrogen Energy*, **14**, 319 (1989).
230. A. Jukic, J. Piljac and M. Metikoš-Huković, *J. Molec. Catal. A: Chem.*, **166**, 293 (2001).
231. G. Kreysa and B. Håkansson, *J. Electroanal. Chem.*, **201**, 61 (1986).
232. M. L. Trudeau, J. Y. Huot, R. Schultz, D. Dussault, A. van Neste and G. L. L'Espérance, *Phys. Rev. B*, **45**, 4626 (1992).
233. D. W. Kirk, S. J. Thorpe and H. Suzuki, *Int. J. Hydrogen Energy*, **22**, 494 (1997).
234. L. Roué, D. Guay and R. Schultz, *J. Electroanal. Chem.*, **455**, 83 (1988).
235. H. Ezaki, T. Nambu, M. Morinaga, M. Udaka and K. Kawasaki, *Int. J. Hydrogen Energy*, **21**, 877 (1996).
236. P. W. Lu and S. Srinivasan, *J. Appl. Electrochem.*, **9**, 269 (1979).
237. S. W. Bushnell and P. M. Purkis, *Chem. Ind.*, 61 (1984).
238. C. L. Linkous, H. R. Anderson, R. W. Kopitzke and G. L. Nelson, *Int. J. Hydrogen Energy*, **23**, 525 (1998).
239. (a) M. Motone, Y. Kawami, Y. Nishimura, M. Mizuhata, K. Oguro and H. Takenaka, *Denki Kagaku*, **62**, 71 (1994); (b) M. Motone, Y. Nishimura, M. Mizuhata and K. Oguro, *Denki Kagaku*, **62**, 425 (1994).
240. P. Millet, R. Durand and M. Pineri, *Int. J. Hydrogen Energy*, **15**, 245 (1990).
241. F. Andolfatto, R. Durand, A. Michas and P. Stevens, *Int. J. Hydrogen Energy*, **19**, 421 (1994).
242. M. Kondoh, Y. Yokoyama, C. Inazumi, S. Maezawa, F. Fujiwara, Y. Nishimura, K. Oguro and H. Takenaka, *J. New Mater. Electrochem. Syst.*, **3**, 61 (2000).
243. K. Ledjeff, A. Heinzel, V. Peinecke and F. Mahlendorf, *Int. J. Hydrogen Energy*, **19**, 453 (1994).
244. Y. Nishimura, K. Yasuda, Z. Siroma and K. Asaka, *Denki Kagaku*, **65**, 1122 (1997).
245. G. Fiori and C. M. Mari, *Int. J. Hydrogen Energy*, **12**, 159 (1987).
246. A. J. Appleby and G. Crépy, 'Electrode Materials and Processes for Energy Conversion and Storage', J. D. E. McIntyre, S. Srinivasan and F. G. Will (Eds), The Electrochemical Society, Princeton, p. 382 (1977).
247. H. Vandenborre, R. Leysen, H. Nackaerts and P. Van Asboreck, *Int. J. Hydrogen Energy*, **9**, 277 (1984).
248. I. Abe, T. Fujimaki and M. Matsubara, *Int. J. Hydrogen Energy*, **9**, 753 (1984).
249. F. Buteau, P. Demange, C. Moreau, R. Gros-Bonnivard and J. M. Jud, *Int. J. Hydrogen Energy*, **18**, 727 (1993).
250. M. Schriber, G. Lucier, J. A. Ferrante and R. A. Huggins, *Int. J. Hydrogen Energy*, **16**, 373 (1991).
251. M. V. Perfiliev, *Int. J. Hydrogen Energy*, **19**, 227 (1994).
252. H. Wendt and G. Imarsio, *J. Appl. Electrochem.*, **18**, 1 (1988).
253. G. B. Barbi and C. M. Mari, *Solid State Ionics*, **6**, 341 (1982).
254. G. Dietrich and W. Schäfer, *Int. J. Hydrogen Energy*, **9**, 747 (1984).
255. L. J. Olmer, J. C. Viguie and E. J. L. Schouler, *Solid State Ionics*, **7**, 23 (1982).
256. G. B. Barbi and C. M. Mari, *Solid State Ionics*, **15**, 335 (1985).
257. G. B. Barbi and C. M. Mari, *Solid State Ionics*, **9**, 979 (1983).

258. T. Ohta, J. E. Funk, J. D. Porter and B. V. Tilak, *Int. J. Hydrogen Energy*, **10**, 571 (1985).

259. A. Lasia, 'Current Topics in Electrochemistry', Research Trends, Trivandrum, India, Vol. 2, 239 (1993).

260. B. E. Conway and L. Bai, *J. Electroanal. Chem.*, **198**, 149 (1986).

261. E. Lamy-Pitara and J. Barbier, *J. Electroanal. Chem.*, **416**, 47 (1996).

262. P. K. Wrona, A. Lasia, M. Lessard and H. Ménard, *Electrochim. Acta*, **37**, 1283 (1992).

263. K. Gossner and F. Mansfeld, *Z. Phys. Chem. N. F.*, **58**, 19 (1968).

264. T. Ohmori and M. Enyo, *Electrochim. Acta*, **37**, 2021 (1992).

265. L. Peraldo Bicelli, C. Romagnani and M. Rosania, *J. Electroanal. Chem.*, **63**, 238 (1975).

266. M. B. Abd Elhamid, B. G. Ateya, K. G. Weil and H. W. Pickering, *J. Electrochem. Soc.*, **147**, 2148 (2000).

267. S. P. Shavkunov, I. N. Sherstobitova and V. V. Kuznetsov, *Elektrokhimiia*, **19**, 816 (1983).

268. M. R. Gennero de Chialvo and A. C. Chialvo, *Phys. Chem. Chem. Phys.*, **3**, 3180 (2001).

269. J. de Carvalho, G. Tremiliosi Filho, L. A. Avaca and E. R. Gonzalez, *Int. J. Hydrogen Energy*, **14**, 161 (1989).

270. A. A. Tanaka, E. R. Gonzalez and L. A. Avaca, *Int. J. Hydrogen Energy*, **11**, 455 (1986).

271. V. M. Tsionskii and L. B. Kriksunov, *J. Electroanal. Chem.*, **204**, 131 (1986).

272. D. Schönfuß, H.-J. Spitzer and L. Müller, *Russ. J. Electrochem.*, **31**, 930 (1995).

273. L. Bai, *J. Electroanal. Chem.*, **355**, 37 (1993).

274. L. Bai, D. A. Harrington and B. E. Conway, *Electrochim. Acta*, **32**, 1713 (1987).

275. L. Huang, F. Yang, S. Xu and S. Zhou, *Trans. IMF*, **79**, 136 (2001).

276. H. Dumond, P. Los, L. Brossard and H. Ménard, *J. Electrochem. Soc.*, **141**, 1225 (1994).

277. Y. Choquette, L. Brossard, A. Lasia and H. Ménard, *Electrochim. Acta*, **35**, 1251 (1990).

278. A. Cornell and D. Simonsson, *J. Electrochem. Soc.*, **140**, 3123 (1993).

279. N. Spãrtaru, J.-G. Le Hellico and R. Durand, *J. Appl. Electrochem.*, **26**, 397 (1996).

280. J. C. F. Boots and S. Trasatti, *J. Appl. Electrochem.*, **19**, 255 (1989).

281. M. J. de Giz, G. Tremiliosi-Filho, E. R. Gonzalez, S. Srinivasan and A. J. Appleby, *Int. J. Hydrogen Energy*, **20**, 423 (1995).